Recent Advances in the Chemistry of Benzo[e][1,2,4]triazinyl Radicals

Fergus J. M. Rogers,[a] Philip L. Norcott [a] and Michelle L. Coote* [a]

*

Benzo[e][1,2,4]triazinyl, or Blatter radicals, are stable free radicals, first reported by Blatter in 1968. In contrast to their nitroxide counterparts, their properties can be modified more widely and more easily through simple substitution changes. This, together with recent developments in their synthesis, now places them at the forefront of developing applications in functional materials. Herein, we survey the various methods to synthesise and customise Blatter radicals, highlighting key developments in the last decade that have transformed their utility. We then outline their important spectroscopic, structural, electrochemical, magnetic and chemical properties and how these depend on their chemical structure and morphology. Finally, we review their growing list of applications including as sensors, spin labels, magnetic materials, liquid crystals and in polymer and small molecule synthesis.

1. Introduction

Radicals that are sufficiently long-lived to be purified and handled earn the special, catch-all moniker, *stable*.[1] In almost all examples of such compounds, the unpaired electron is resonance stabilised or sterically protected, being confined to a rigid, often lone-pair rich molecular backbone. Discussions on radical stability have been given elsewhere,[2] however we note that these properties stabilise the *singly occupied molecular orbital* (SOMO) toward radical deactivation, with rare examples surviving decades under ambient conditions before noticeable degradation.
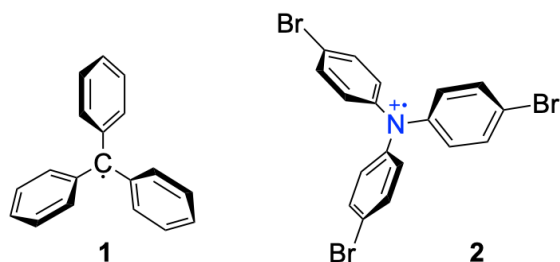

Figure 1. The triphenylmethyl or *trityl* radical (*left*) and its *N*-centred triarylammonium radical cation (*right*).

Only relatively few classes of stable radicals have been reported since Gomberg's publication of the prototypical "persistent", *i.e.* visible by electron paramagnetic resonance (EPR), triphenylmethyl radical **1** in 1900 (Figure 1).[3] The nitrogen analogues, such as the commercially available salt **2**, form radical cations which are among the simpler examples exhibiting bench stability.[4-7] This may be enhanced through steric protection or π-system overlap into the adjoining arene substituents,[8] for example, the ether bridged species **3**[9] and the elegant, sterically-protected analogue **4** (Figure 2).[10]
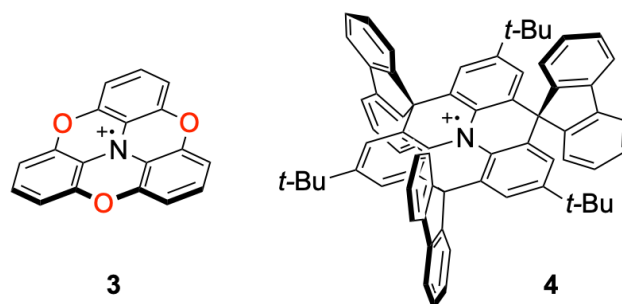

Figure 2. Stabilised triarylammonium radical cations.[9,10]

Arguably the most well-known family of stable radicals are the nitroxides (or *aminoxyl* radicals), which are of the general form $R_2NO^{\bullet}$. Here, the unpaired electron resides in a π^* orbital centred on the NO moiety, resulting in a three-electron interaction exemplified in the two resonance structures of **5** shown in Scheme 1. Nitroxides are typically air- and moisture-stable owing to the thermodynamic penalty of concatenated lone-pair rich atoms. Aliphatic species protected by quaternary α carbons, such as (2,2,6,6-tetramethylpiperidin-1-yl)oxyl (TEMPO) are particularly robust,[11] having found use as reporter molecules in EPR[12,13] and mechanistic studies,[14,15] catalytic oxidation,[16,17] polymer chemistry,[18-20] and more recently in organic batteries,[21,22] magnetic and "smart" materials, among others.[23-28]
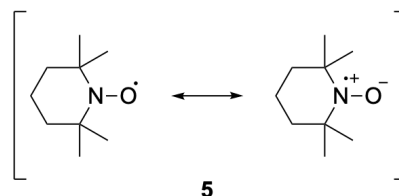
Scheme 1. Resonance stabilization of (2,2,6,6-tetramethylpiperidin-1-yl)oxyl (TEMPO).

Although ubiquitous, nitroxides are certainly not the only class of stable radicals known to the literature. Rigid and fused

hydrazyl radicals, in particular the *verdazyl* radicals (**6,7**) studied by Kuhn and Neugebauer[29-36] and the conventionally named benzo[e][1,2,4]triazinyl, or *Blatter* radicals (**8**), the subject of this review, are classic examples exhibiting exceptional all-round stability (Figure 3). In both species, the unpaired electron is formally centred on a nitrogen atom within a rigid, nitrogen-rich heterocycle. In reality, the SOMO is highly delocalised and therefore sensitive to substituent variations. This property alone is very advantageous, as simple structural modifications can have broad impacts on the ultimate behaviour of the radical.

Kuhn verdazyl: X = CH$_2$ **6**
Oxoverdazyl: X = CO **7**
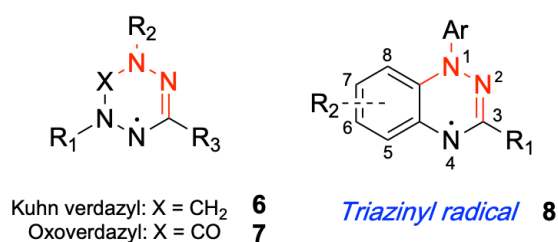
Triazinyl radical **8**

Figure 3. Generalised verdazyl and Blatter radicals with numbering scheme assumed in this work. The hydrazyl moiety common to both structures is highlighted in red.

Blatter radicals have only gained traction in recent years but are now abundant in the broader scope of stable-radical chemistry. Herein we provide an overview of this progress, discussing preparative routes and derivatisation, basic properties and functional scope. Throughout the text, we make frequent use of radicals **9** and **10** (Figure 4). The synthesis and analysis of **10** is described in the Supporting Information, where readers will also find computational methodology and other aspects related to modelling undertaken in this report. As for existing literature, Koutentis and Constantinides have previously discussed Blatter radicals as part of an instructive book chapter,[37] whilst their role in devices and other technologies was very recently reviewed by Zheng *et al.*[38] Magnetic properties have also been described in a broader outline on the topic by Mukhopadhyay *et al.*[39] As usual, direction will be made to these articles when appropriate.
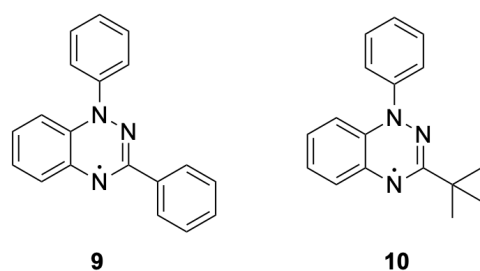

Figure 4. Radicals frequently referenced in this work.

2. Synthesis

Synthetic strategies for Blatter radicals have been developed sporadically since their discovery over fifty years ago to the date of this review.[40] Until recently, preparations were tedious and suffered from various inefficiencies that prohibited their widespread adoption.[31,32,41-43] Thanks to the efforts of various

researchers over the last decade, particularly those of Koutentis, Constantinides and Kaszyński *et al.*,[44-49] access to Blatter radicals has been greatly diversified and now a large library of compounds are known to the literature.

2.1 Early Reports and Syntheses

The first known example of a Blatter radical was described by the eponymous author in a seminal 1968 paper, "A new stable free radical".[40] The compound in question, 1,3-diphenyl-1,4-dihydrobenzo-1,2,4-triazin-4-yl, *Blatter's* radical (**9**), was prepared from a reactive 1,3,4-triphenyl-1,2,4-triazabutadiene, or *azoimine,* **11** (Scheme 2).[50] Upon acidification in hydrogen bromide, this intermediate rapidly cyclised to an isolable 1,4-dihydro or *leuco* triazine salt **12**. Quantitative aerobic oxidation to the radical was completed over several hours in ethanolic potassium hydroxide *via* **13**, although various pathways were noted to form the desired product from the free base of **12**.
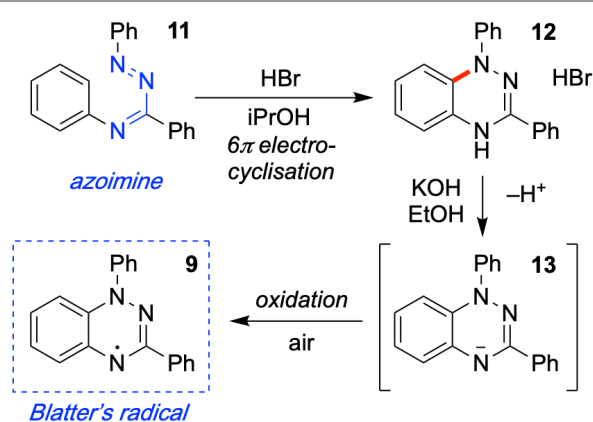

Scheme 2. Blatter's synthesis of the 1,3-diphenyl-1,4-dihydrobenzo-1,2,4-triazin-4-yl radical **9**.[40]

Several unspecified radicals were prepared from various azoimines using this methodology, including the 1-(*p*-tolyl)-6-methyl analogue **17**. In an effort to corroborate Scheme 2, this compound was also synthesised through an alternate pathway, shown in Scheme 3. Here, bromination of *N'*,*N'*-di-(*p*-tolyl)benzohydrazide **14** enabled selective nitration to **15**. Simultaneous reduction of the nitro group and hydrodehalogenation was accomplished under hydrogenative conditions. The resulting amine **16** underwent a cyclodehydration to the leuco form in refluxing ethanol followed by aerobic oxidation under basic conditions to yield the radical **17** in low yield.
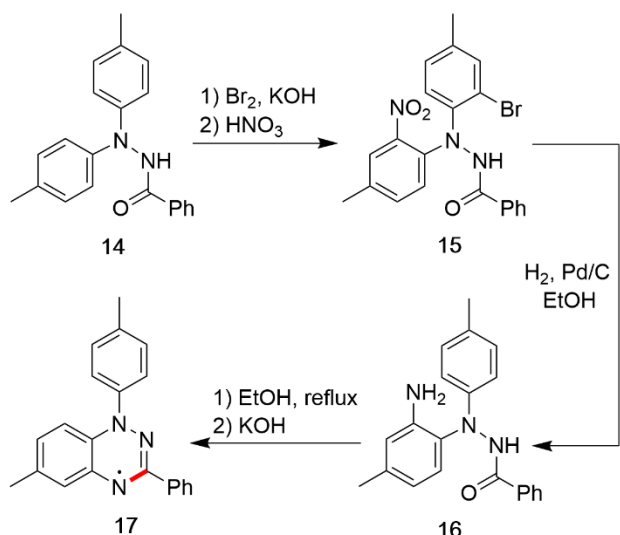
Scheme 3. Blatter's novel preparation of the 1-(p-tolyl)-6-methyl analogue **17**.[40]

Shortly following the publication of Blatter's work, Huisgen and Wulff reported the preparation of the 7-methoxy analogue **21** (where R = OMe) *via* aza-Wittig chemistry (Scheme 4).[51] Here, the addition of diphenylnitrilimine **18** to *N*-(4-methoxyphenyl)-imino(triphenyl)phosphorane **19** resulted in a complex reaction mixture from which a sparing (6%) yield of radical **21** was isolated. Huisgen identified this annulation as an electrocyclic mechanism requiring an intermediate azoimine, in this case generated by the elimination of triphenylphosphine.
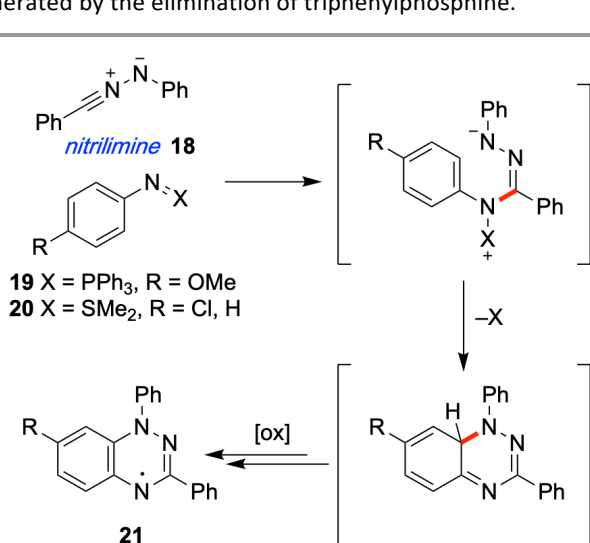

Scheme 4. Aza-Wittig-type approaches to Blatter radical synthesis.[51]

Analogues of **21** (where R = Cl) also formed under an analogous addition of diphenylnitrilimine **18** to sulphur-based aza-ylides (**20**) in dichloromethane (Scheme 4).[52] Partial oxidation to radicals was noted during workup, with isolation of trace azoimine supporting the electrocyclic mechanism as proposed by Huisgen.
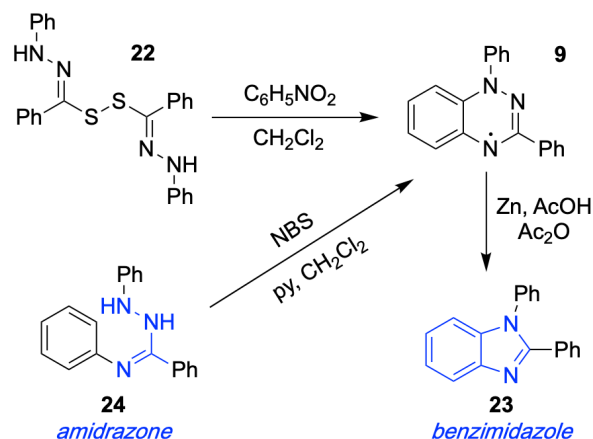

Scheme 5. (*Top*) Formation of Blatter's radical from the oxidation of disulphide **22** with nitrobenzene.[53] (*Left*) One-pot transformation to the radical from the amidrazone, and its reductive ring contraction (*Right*) to 1,2-diphenylbenzimidazole.

Soon after, Magnus *et al.* observed predominately Blatter's radical **9** (24% yield) from the oxidation of disulphide **22** with nitrobenzene (Scheme 5).[53] The reactivity of **9** was studied in the context of a reductive ring contraction to the 1,2-diphenylbenzimidazole **23**. This useful transformation has since been generalised (see Section 2.3). Formation of **9** (74% yield) was also achieved from the addition of *N*-bromosuccinimide to *N'*-phenylbenzhydrazide phenylhydrazone **24**, an *amidrazone* and precursor to the azoimine.
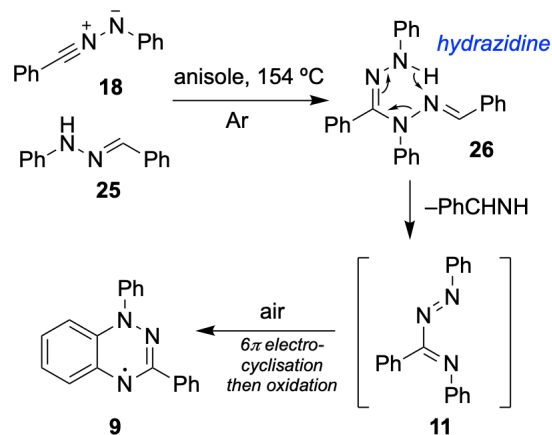
Scheme 6. Proposed formation of Blatter's radical **9** by thermolysis of hydrazidine **26**.[52]

Blatter's radical (**9**) was later observed by Buzykin and Gazetdinova in their analysis of the various products resulting from the addition of diphenylnitrilimine **18**, to benzaldehyde 2-phenylhydrazone **25** in refluxing anisole (Scheme 6).[54] The minor product of this reaction, the *hydrazidine* **26**, underwent thermolysis forming the intermediate azoimine **11**, and the subsequent radical **9** under air.
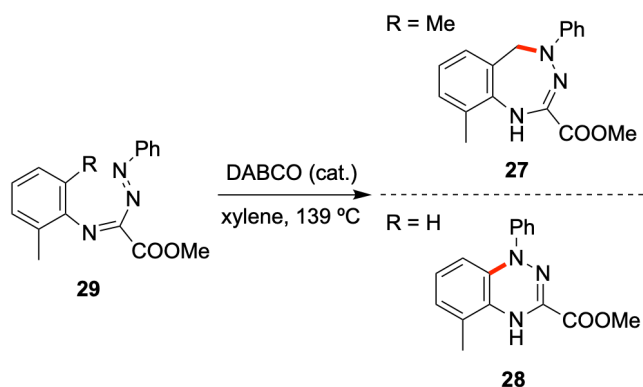
Scheme 7. Thermal cyclization of azoimines to benzotriazepines.[54]

Finally, during a preparative study of the dihydrobenzotriazepine 27 by Sannicolo *et al.* (Scheme 7),[55,56] leuco triazine 28 was identified as the major product (62% yield) from the thermal cyclization of azomine 29 (where R = H) in the presence of catalytic 1,4-diazabicyclo[2.2.2]octane (DABCO). In this case, alkylation of both *ortho* positions (compound 19 where R = Me) was necessary to block the competitive electrocyclic pathway.
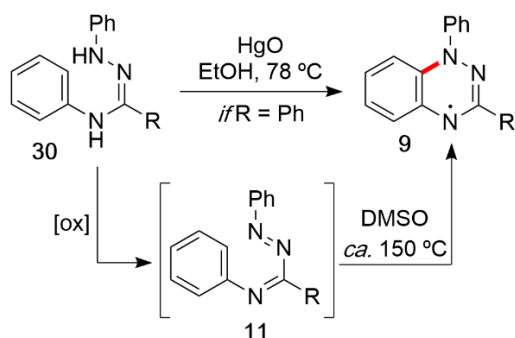

Scheme 8. Neugebauer's general synthesis of Blatter radicals from amidrazones.[41]

Blatter radicals were not re-examined in great detail until Neugebauer and Umminger in the early 1980's,[41] who described a general preparation involving thermal cyclisation of the azoimine in dimethylsulfoxide, before further oxidation to the radical with metallic oxides (Scheme 8). Buzykin separately reported this transformation in refluxing anisole.[54] A number of new radicals were prepared under these conditions, including a series of 3-*tert*-butyl examples as well as a selection of deuterated analogues. Interestingly, oxidation of amidrazone (R = Ph) in boiling ethanol afforded Blatter's radical directly (51%), quite analogous to the one-pot transformation of this species reported by Magnus.[53] These conditions were not found to be generally applicable however (*vide infra*).

2.2 Recent Developments

Neugebauer's product-specific preparation of Blatter radicals suffered from several inefficiencies connected to isolation of the unstable azoimine.[41] This was often used in crude form, hampering efforts to boost the overall yield of the radical. Clearly, direct transformation from the amidrazone would resolve these problems and had already been shown for

Blatter's radical in the presence of oxidants,[41,53] but this method was unable to access a broader scope of triazinyl radicals.
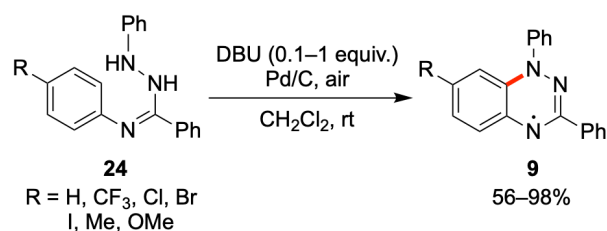
Scheme 9. Koutentis's popular one-pot adaptation of scheme 8.[44]

Koutentis *et al.* were the first to arrive at a solution. Screening a selection of oxidants and bases, they discovered that a combination of 1,8-diazabicyclo[5.4.0]undec-7-ene (DBU, 0.1–1 equivalents) and palladium-on-carbon (1.6 mol%) in air, facilitates a rapid conversion of amidrazones to Blatter radicals at room temperature (Scheme 9).[44] Unlike Neugebauer's method however, which relied on expensive or toxic metal oxidants and moderate heating, these comparatively mild conditions are more efficient, suffering very little over-oxidation to benzotriazin-7-ones (see Section 2.3).
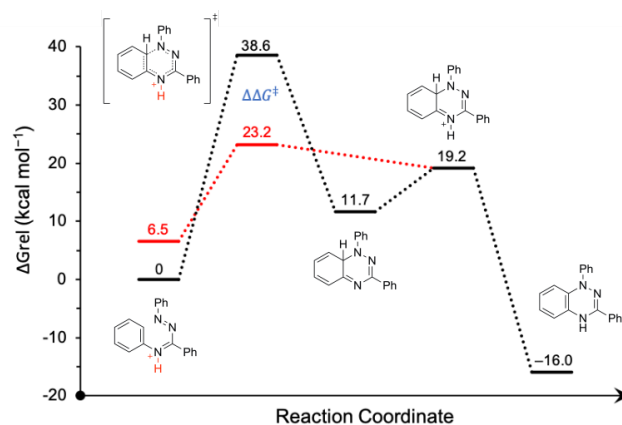

Figure 5. Mechanism for the electrocyclic ring closure of the azomine 11 to the leuco triazine. Effect of protonation by Me₃NH⁺ highlighted in red. Details regarding the modelling can be found in Ref. [57].

Palladium-on-carbon was initially selected for its catalytic role in the aerobic oxidation of alcohols.[58] This is known to be influenced by pH,[59,60] and deprotonation with a base would almost certainly expedite the oxidation of the amidrazone to an azoimine. Indeed, under an atmosphere of oxygen, various organic bases of comparable strength [DBU, pyridine, 4-(dimethylamino)pyridine (DMAP), triethylamine and ethyldiisopropylamine (Hünig's base)] enabled radical formation. Kaszyński *et al.* later calculated that protonation of the azomine decreases the rate-limiting electrocyclisation barrier by some $\Delta\Delta G^{\ddagger} = 15.4$ kcal mol⁻¹ (Figure 5). This would support the formation of radical products at room temperature in the presence of base.[57] Nevertheless, for reasons that are not understood, only DBU managed this transformation under an atmosphere of air and with unusual efficiency (with 98% yield of 9).
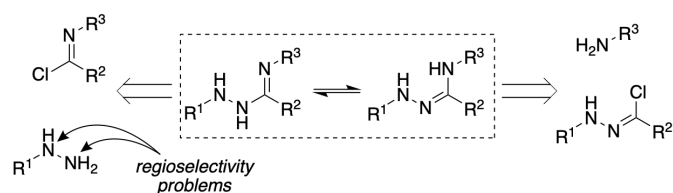
Scheme 10. Synthetic approaches to amidrazones.[57]

Amidrazones are typically prepared by substitution of an imidoyl chloride with an arylhydrazine, or a hydrazonyl chloride with an aromatic amine, the latter being preferred as it eliminates the requirement for regioselectivity in the penultimate step of the synthesis (Scheme 10). These compounds vary in their bench-stability and on silica gel, often requiring immediate use following purification so as to minimise degradation. Purification is critical here as the ultimate yield in radical is sensitive to the quality of the starting material.
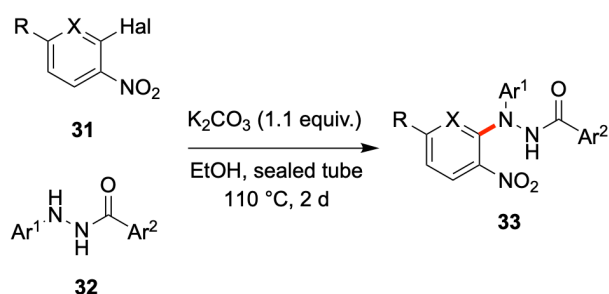

Scheme 11. Access to the nitroaryl-functionalised hydrazides **33**, precursor to the reductive cyclodehydration method.[45]

In the interest of avoiding these temperamental intermediates, Koutentis demonstrated a modification of Blatter's cyclodehydration method (Scheme 3).[45] Unlike Blatter's preparation however, which involved an inefficient protection strategy to selectively access the nitro-functionalised hydrazide **15**, these key intermediates may be prepared directly by nucleophilic aromatic substitution of halide **31** with hydrazide **32**, giving the coupled product **33** (Scheme 11). Although more general and efficient, some difficulty arose in the preparation of hydrazides with non-aryl substituents at Ar[2]. This limitation can be met with protecting group chemistry, however.
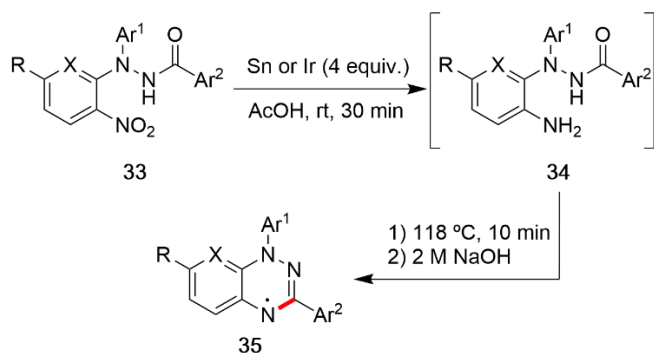

Scheme 12. One-pot reductive cyclodehydration strategy of **33** to Blatter radicals.[45]

Mild reduction of the nitro group of **33** followed by acid-mediated cyclodehydration results in the oxidatively-unstable leuco triazine. Alternatively, this can be accomplished in one pot with excess (4 equivalents) metallic reducing agents to give **34**, followed by cyclisation and oxidation to radical **35** (Scheme 12). Tin and indium were the most effective choices based on an optimisation screen, particularly in comparison to iron. In agreement with Magnus,[53] more aggressive metal reductants, such as zinc or copper, facilitated an irreversible, reductive ring contraction of the desired radical to a benzimidazole (as in Scheme 5).
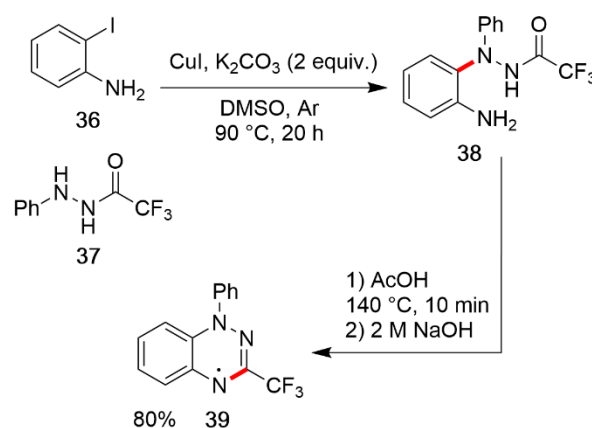
Scheme 13. Copper-mediated C–N coupling protocol toward radical **39**.[46]

Based on the work of Ma et al.,[61] the transformation in Scheme 11 was later modified to a copper-mediated C–N coupling, with 2-iodoaniline **36** and hydrazide **37** (Scheme 13), thus avoiding the additional reduction step to reach amine **38**. This adaptation is more compatible with alkyl groups at C3, eliminating the need for protecting group chemistry. For example, the 3-trifluoromethyl radical **39** could be prepared in 80% yield, a marked improvement on the 37% procured via Scheme 11.[46]
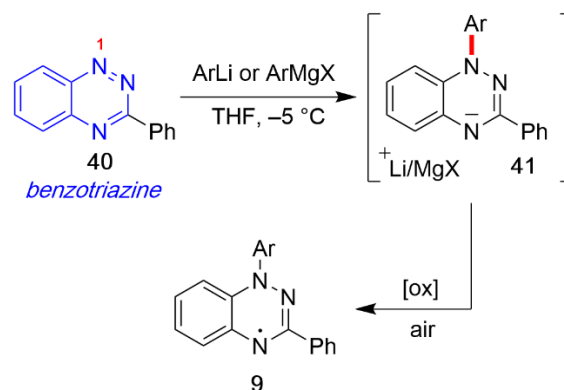
Scheme 14. Azaphilic addition of organometallic reagents to benzotriazines.[47]

Functionalisation at the N1 position is ordinarily limited by the accessibility of the antecedent arylhydrazine. As a means to expand the substrate scope at this position, Kaszyński et al. then explored the synthesis of Blatter radicals through the azaphilic addition of organolithium or Grignard reagents to *benzotriazines* **40** (Scheme 14).[47] Addition initially forms a

stable triazinyl anion **41**, which slowly oxidises to the radical upon exposure to air. Analysis of the Fukui functions supported regioselective addition to N1;[62] this was observed in all examples. Readers should note the slight instability of electron-rich radicals on solid supports, for example the 7-methoxy species (Ar = 2-methoxyphenyl). Nevertheless, purification of this compound has been accomplished by direct crystallisation or through trapping of the anionic intermediate with electrophiles.[63]
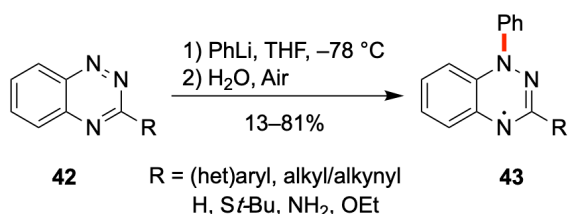

Scheme 15. Addition of phenyllithium to various 3-functionalised benzotriazines in Ref. [64].

Depending on the stability of the aryllithium reagent, it may also be necessary to generate this key component *in situ*, that is, through metal-halogen exchange or direct lithiation in tandem with azaphilic addition. Sensitive functional groups, such as halogens or competitive acceptors such as carbonyl-containing groups, are not expected to perform adequately in these systems, adding some limitations to the preparative scope of Scheme 14. This said, recent developments in benzotriazine synthesis has enabled access from **42** to a variety of novel, 3-functionalised Blatter radicals (**43**, Scheme 15),[64,65] not easily accessible by any alternative method discussed here.
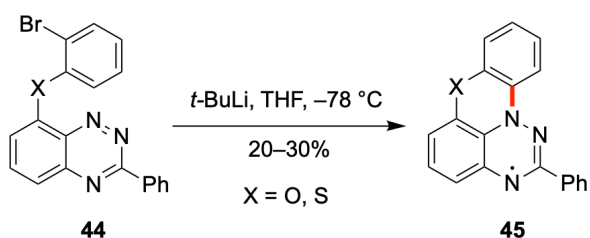

Scheme 16. Intramolecular azaphilic addition to form planar Blatter radicals.[66]

Planar radicals in which the aryl substituent at N1 is joined by a chalcogen bridge to C8, have also been prepared through an intramolecular version of this reactivity (Scheme 16).[66] After an initial lithium-halogen exchange, 8-(2-bromo)phenoxide and thiophenoxide-functionalised benzotriazines **44** undergo an intramolecular azaphilic addition to N1, forming the planar analogues of Blatter's radical (**45**). Alternate coupling mechanisms, including radical Pschorr-type annulation and a promising photocyclisation route have since been proposed (Scheme 17).[67,68] These strategies have greatly broadened the variety of planar radicals in the current literature.
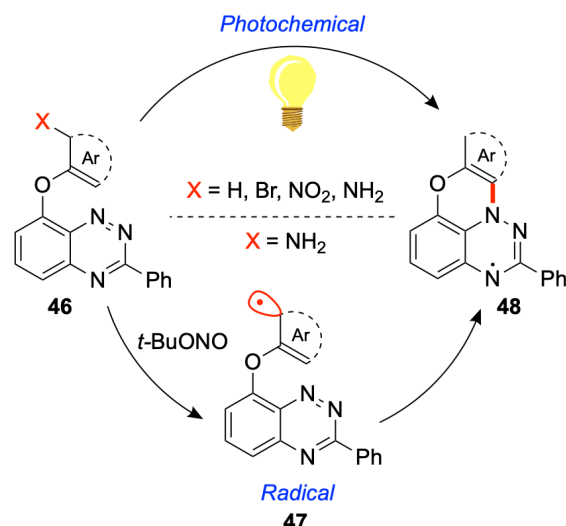
Scheme 17. New methods towards the preparation of planar Blatter radicals.[67,68] Note: the authors also described the ring closure of the N-nitrosylated precursor (Y = NAcNO) with metallic zinc.

Chechik and O'Donoghue *et al.* later documented the one-pot transformation of the nitron **49** to the 3-amidyl radical **50** via *N*-formyl intermediate **51** in wet acetonitrile (< 10% v/v).[48] This surprising discovery facilitated the synthesis of the 3-anilino derivative **52**; the first examples of Blatter radicals with nitrogen-based substituents at C3 (Scheme 18). Other analogues were prepared from a variety of nitrons, demonstrating the scope of this transformation.
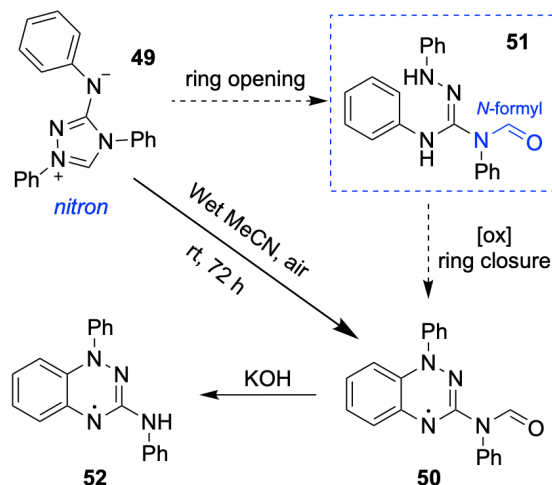
Scheme 18. Spontaneous transformation of nitron **30** to the 3-amidyl radical **32** in wet acetonitrile.[48]

The rearrangement of **49** occurs through an initial hydrolytic ring opening to an *N*-formylated amidrazone **51**. The exocyclic nitrogen appears to be essential here as a solution of 1,3,4-triphenyl-1,2,4-triazolium tetrafluoroborate **53** (which ought to form Blatter's radical), remained unchanged under analogous conditions (Scheme 19). Further transformation to the radical might simply result from an intermediate azoimine, however the authors speculated that a hydrazonyl radical could also accomplish annulation. Interestingly, high water concentrations

(50%) favoured the formation of the 3-anilino azoimine **54**, also predominate in basic, degassed acetonitrile (Scheme 19). Thus, whilst the presence of water provides selective access to the *N*-formylated amidrazone, subsequent formation of the radical appears to be competitive with hydrolysis to **54**, which does not undergo further conversion to radical **52**. This implicates the key role of the formyl group in completing the transformation, possibly through a subtle inductive effect, although the exact reasons for this remain to be investigated in greater detail.
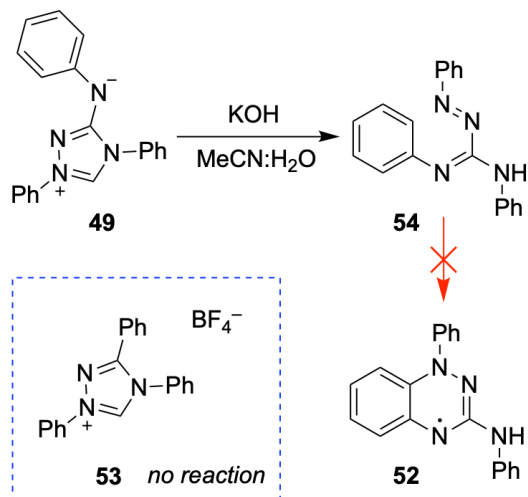
Scheme 19. Preferential formation of **54** in degassed acetonitrile and aqueous potassium hydroxide. (*Boxed*) Triazolium salt **53** fails as a direct precursor to Blatter's radical.[48]

Inspired by the pioneering work of Huisgen (Scheme 4),[51] Koutentis *et al.* finally re-examined the aza-Wittig pathway toward the preparation of Blatter radicals.[49] Rather than engaging a nitrilimine, *diazenes* (**55**) were identified as more reliable substrates for the synthesis of radicals in combination with *N*-aryl-imino(triphenyl)phosphoran*es* (**56**), generating radicals of the form **57** (Scheme 20).
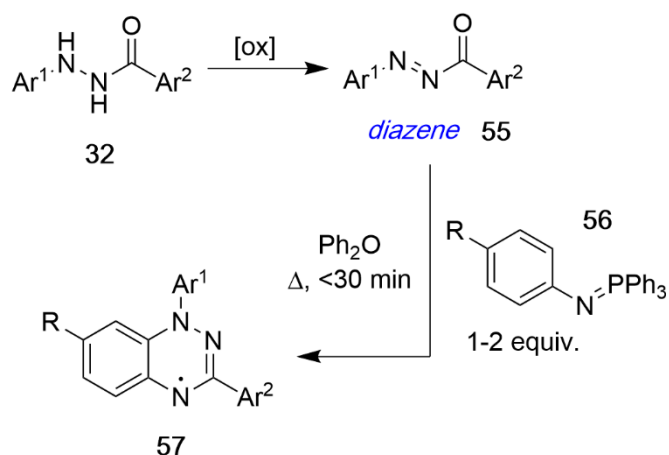
Scheme 20. Revised aza-Wittig preparation of Blatter radicals via a diazene intermediate.[49] Depending on the substrate, a range of oxidising agents were utilised including powdered HgO in n-hexane, NaNO$_2$ (3 equiv)/Ac$_2$O (3 equiv) and NBS (1 equiv) and pyridine (1.1 equiv) in CH$_2$Cl$_2$, see Ref 49 for more details.

After the initial aza-Wittig reaction to form an azoimine, transformation to the radical presumably follows the electrocyclic mechanism of Figure 5. In many cases however, the high reaction temperatures needed to accomplish this step resulted in the appearance of benzotriazin-7-ones (Sec 2.3). This could be suppressed under air-free conditions, however the 4-methoxyphenyl and 4-nitrophenyl derivatives (**56**, R = OMe, NO$_2$) both gave mainly the over-oxidised species, despite efforts to eliminate oxygen. Excess iminophosphorane (up to 2 equivalents) was also found to improve yields in most examples, likely through limiting the competitive decomposition pathways of the diazene. These intermediates could not be prepared from acetyl, trifluoroacetyl and pyridine-2-carbonyl hydrazides, which oxidised to complex reaction mixtures, limiting scheme 20 to the synthesis of radicals **57** with aryl substituents at C3.
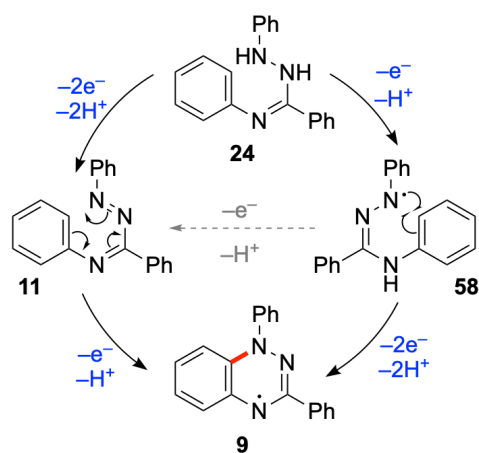

Figure 6. Mechanistic considerations for the oxidative annulation of amidrazones.[48] For the sake of brevity, tautomerisations and conformations are excluded from this scheme.

Schemes 9, 18 and 20 ostensibly involve the *in situ* formation of an azoimine, the key component in the electrocyclic formation of Blatter radicals. Kaszyński's modelling determined that this ought to be assisted by acid catalysis (Figure 5). One might then expect some improvement to Scheme 20 under such a modification, however no change was observed with Bronsted and Lewis acids in either catalytic (5 mol%) or stoichiometric amounts (100 mol%). Alternatively, ring activation could be conducted by a hydrazonyl radical **58** (Figure 6). Indeed, the isolation of azoimines does not preclude the intermediacy of this species.[48] Clearly, the formation of Blatter radicals from amidrazones is not fully understood and deserves further study.

2.3 Functional Group Transformations

Benzotriazin-7-ones **59** are the most prevalent oxidation product of Blatter radicals.[69,70] Typically undesirable, their formation is essentially eliminated by placing non-labile substituents at C7, for example the "super stable" 7-trifluoromethyl analogue of Blatter's radical.[71] Although a by-product in the preparations described, these compounds have been shown to undergo selective addition of nucleophiles and electrophiles at C6 and C8, respectively.[72] This chemistry has been put to use in synthesis in a number of contexts, including towards medicinally relevant compounds.[73,74] More relevant

however, is their use in the preparation of a series of heterole-fused radicals of the form **60** (Scheme 21).[75,76]
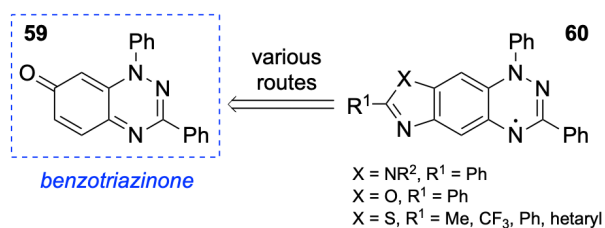
Scheme 21. Access to the π-extended radicals (**60**) from benzotriazin-7-one **59**.[75,76]

Access to the leuco triazine is easily achieved with mild reducing agents such as ascorbic acid.[57] Most examples are of course unstable to molecular oxygen or mild oxidants (*e.g.* sodium periodate), rapidly reforming the radical on the bench. As mentioned previously, stronger reducing agents, *i.e.* metallic zinc, facilitate an irreversible, reductive ring contraction to a benzimidazole. This behaviour in radicals of the form of **61** has been optimised by Koutentis *et al.* as a route for accessing 1,2-diphenylbenzimidazoles (**62**),[77] particularly the asymmetrical heterole-fused species for which alternate preparations are sparse.[78] Influenced by the early observations of Magnus *et al.*,[53] radicals are heated to reflux in glacial acetic acid with excess zinc powder, forming the desired products in near-quantitative yields (Scheme 22). This reductive method (albeit from a relatively advanced precursor) complements the traditional strategies to form 1,2-disubstituted benzimidazoles, which are typically cyclocondensation or oxidative processes, or cross-dehydrogenative couplings.[79]
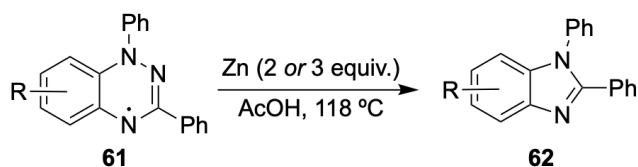
Scheme 22. Reductive ring contraction of Blatter radicals (**61**) to 1,2-diphenylbenzimidazoles (**62**).[77]

Very few stable radicals are known to participate in palladium-catalysed cross-coupling reactions. Among early reports were the Heck, Suzuki-Miyaura and Sonagoshira-type couplings of bromide and iodine functionalised nitronyl nitroxides, respectively.[80-82] Motivated by these results, Koutentis *et al.* were the first to explore the viability of halogenated Blatter radicals (**63**) as substrates in Stille and Suzuki-Miyaura-type reactions to access **64** (Scheme 23).[83] Readers should also note the recent extension of this chemistry to the verdazyl radicals, which are yet to experience equal success.[84,85]
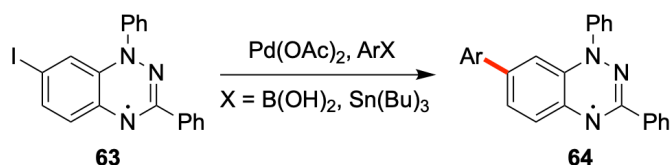
Scheme 23. Suzuki-Miyaura and Stille cross-couplings with Blatter radicals (note; other Pd catalysts and conditions were tested).[83]

For the Stille reaction, yields up to 78–93% were achieved with the use of two equivalents of aryl stannane, whilst three equivalents of aryl boronic acid was most efficient for the Suzuki reaction, which also achieved yields of 67–93%. Naturally, not all substrates performed equally under the standard conditions; only moderate conversions or complex reaction mixtures were experienced with electron deficient boronic acids. However, these may prove to be feasible utilising alternative borane or catalyst combinations in future studies. Radical derivatives **65** and **66** have subsequently also been prepared using Suzuki-Miyaura and Stille reactivity, respectively (Figure 7).
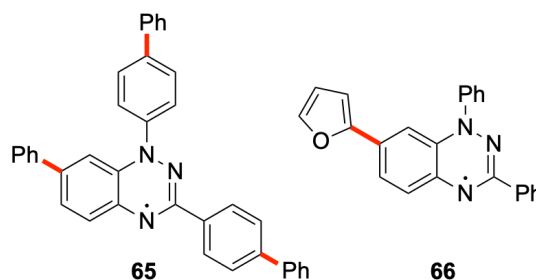
Figure 7. Derivatives prepared in Suzuki-Miyaura (*left*) and Stille (*right*) cross-coupling reactions with iodine-functionalised Blatter radicals; relevant bonds formed highlighted in red.[86,87]

In terms of general derivatisation, Kaszyński's authoritative study on Blatter radicals is most instructive (Figure 8).[57] For the sake of completeness, we briefly describe some selected examples of this work here, but urge readers to address the full article for a deeper understanding of Blatter radical chemistry.

R^1, R^2 = OBn, OBz, NO$_2$, I, CO$_2$Me
R^3 = H, 7-CF$_3$, 6-CF$_3$, 7-I
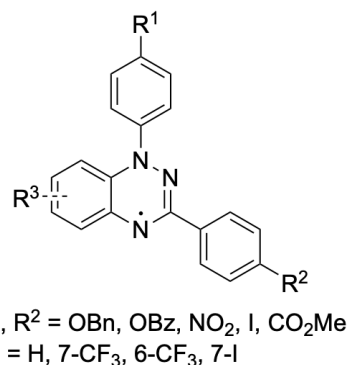
Figure 8. Radicals examined as substrates for derivatisation in Ref. [57].

Basic hydrolysis of benzoate functionalised radicals was first demonstrated by the rapid and quantitative deprotection of **67** to the bisphenol species **68** (Scheme 24). Alkylation was subsequently attempted with varying success on phenol derivatives under standard conditions. To this end, it was found that **68** reacted successfully with 1-adamantanecarbonyl chloride forming the diester **69** in 91% yield. Hydroxy substituents were also accessible through hydrogenation of the corresponding benzyl ether, with the use of both options giving scope for orthogonality. Furthermore, carboxylic acid-functionalised radicals were obtainable by hydrolysis of the corresponding methyl esters.
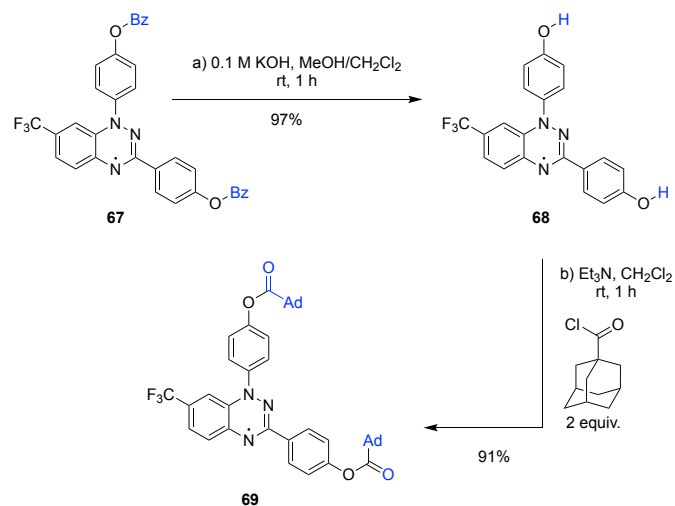
Scheme 24. Ester hydrolysis of **67** to the bisphenol radical **68** and subsequent esterification to **69**.[57]

Building on the work of Koutentis *et al.*,[83] various iodine functionalised radicals were examined for many of the remaining palladium-catalysed cross-coupling reactions. Once again, most examples including Sonogashira and Heck couplings performed well, however the Negishi reaction of **70** with (4-methoxyphenyl)zinc bromide (Scheme 25), suffered from comparatively poor yields of radical **71** (46%) and the appearance of the leuco form by thin-layer chromatography.
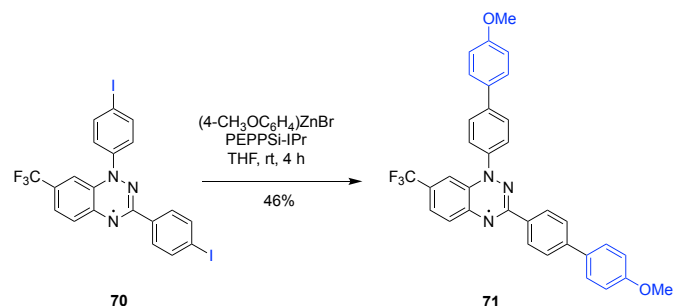
Scheme 25. Negishi reaction of **70** with (4-methoxyphenyl)zinc bromide.[57]

Finally, catalytic hydrogenation of the 3-(4-nitrophenyl) functionalised radical **72** to the aniline derivative **73** was performed quantitatively over palladium-on-carbon. This new radical, isolated in 98% yield, was coupled to *N*-Boc-protected L-proline, forming the biochemically relevant amide **74** (Scheme 26). By comparison, attempts at reductive amination with hexanal could not be driven to completion.

Scheme 26. Preparation of biochemically relevant Blatter **74** from the 3-(4-nitrophenyl) precursor **72**.[57]

3. General Properties
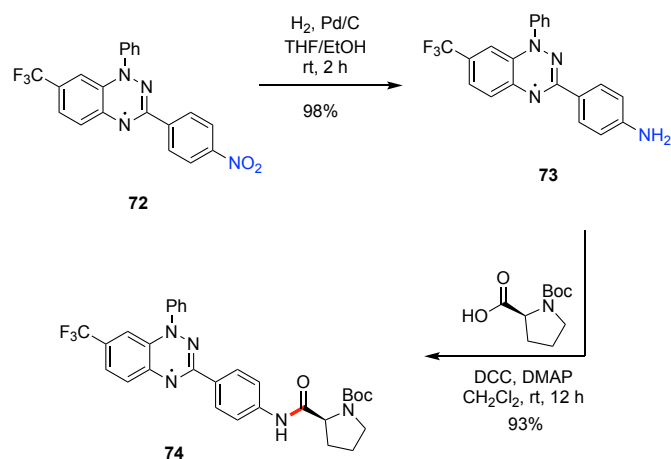
3.1 Spectroscopic

The UV/Vis absorption profile for dilute Blatter radicals typically consists of one major absorption in the UV region, followed by a sequence of minor adsorptions trailing into the visible region (Figure 9). *Time-dependent density functional theory* (TD-DFT) calculations have been conducted by several authors in order to characterise these features.[57,64,88] While the major absorption in the UV region can be attributed to a predominately HOMO-1 to LUMO transition, the SOMO to LUMO transition is barely visible in most examples due to its low oscillator strength, a result of poor SOMO-LUMO overlap.
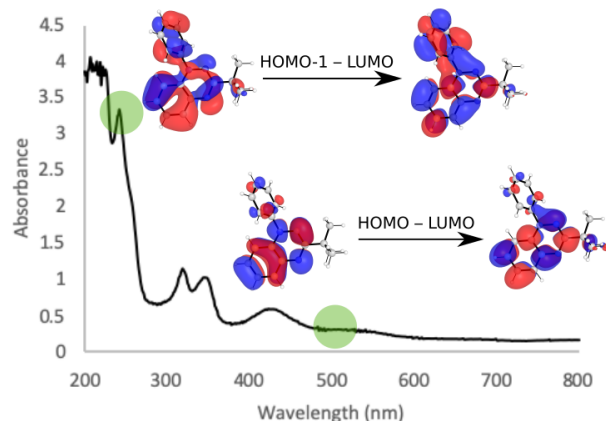
Figure 9: Raw absorption spectrum of radical **10** (0.1 mM) in dichloromethane. Selected natural transition orbitals are shown, these are described in the Electronic Supplementary Information.

Fluorescence emission studies of Blatter's radical **9** have also been conducted by Itskos and Hayes *et al*.[88] Under UV (270 nm) excitation in the solution phase, a strong and narrow emission band was measured at 350 nm. This mirrors the major absorption observed at this wavelength (Figure 10). Interestingly, broad, stoke shifted features in the visible region was observed under excitation between 430 and 550 nm,

indicative of internal conversions to the LUMO prior to emission. Most noteworthy here was the broad white-light emission measured under ~370 nm excitation, a rare property among organic molecules useful in the design of light-emitting devices.[89] Some work is needed to improve its fluorescence quantum yield in the visible region however, with the authors noting that derivatisation could offer recourse.
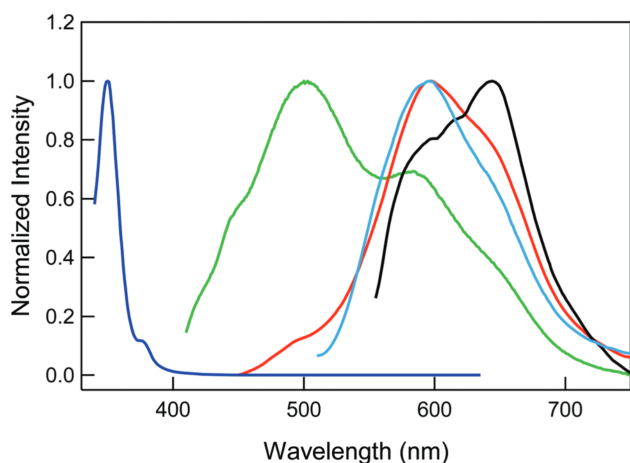
Figure 10. Fluorescence emission spectra of Blatter's radical **9** (0.1 mM) in dichloromethane under 270 nm (Blue), 370 nm (Green), 430 nm (Red), 490 nm (Blue) and 550 nm excitation (Black). Reproduced with permission from Ref. [88]. Copyright (2017) Royal Society of Chemistry.

Time-resolved fluorescence decay with 500, 590 and 650 nm excitation was subsequently measured for **9** in the solution and solid phases. These indicated average lifetimes of 2–3 ns in dichloromethane, with greater variation in thin films (1.5–5 ns) and shorter lifetimes in 50:50 radical:polymethylmethacrylate blends (1–1.5 ns). Optical properties relating to the unpaired electron typically diminished in solutions or films above a certain concentration. This effect can be attributed to dimer radical aggregation and should be manageable with steric modifications to **9**. Incidentally, these studies indicated dichloromethane as the best solvent choice for this species.

3.2 Electron paramagnetic resonance (EPR)

EPR studies of Blatter's radical were initially conducted by Neugebauer and Kadirov in the 1980s. Beyond conventional continuous-wave (CW-EPR) measurements,[42] isotope labelling, double electron-nuclear resonance (DENR),[90] electron nuclear double resonance (ENDOR) and triple resonance spectra have been obtained for **9**.[43] Few other radicals have been studied in similar detail. These include the 3-*tert*-butyl (**10**)[43] and the 1-(4-nitrophenyl) analogues.[91]
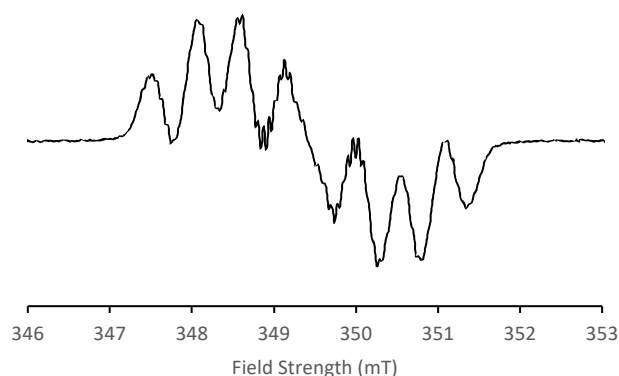
Figure 11. CW-EPR spectrum of **10** in toluene. Experimental details and simulation described in the Electronic Supplementary Information.

The spectral composition of Blatter radicals is primarily characterised by seven principle lines, consistent with coupling of the unpaired electron to three nearly equivalent quadrupolar ^{14}N nuclei (Figure 11). In terms of hyperfine coupling constants (hfcc), the greatest share in spin-density generally resides at N1, followed by N4 then N2, in no particular order.
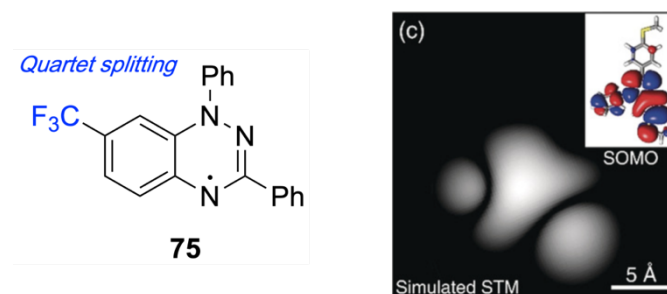
Figure 12. (*Left*) Source of further splitting in the spectrum of **75**.[71] (*Right*) SOMO surface of a typical Blatter radical. Reproduced with permission from Ref. [92]. Copyright (2019) John Wiley & Sons, Inc.

The presence of spin-active heteroatoms, typically at C3 and C7, causes further splitting in the resultant spectrum. For example, the 7-trifluoromethyl radical **75** (Figure 12) is characterised by twelve principle lines as opposed to seven, resulting from additional hyperfine coupling (3.45 G) to three equivalent ^{19}F nuclei.[71] A similar effect is observed in the 3-trifluoromethyl analogue, only with a smaller hfcc (1.89 G),[45] whilst the effect at N1–Ar tends to be negligible given that the substituent is essentially perpendicular to the heterocycle (note: a considerable increase is observed in the planar radicals studied by Kaszyński *et al.*).
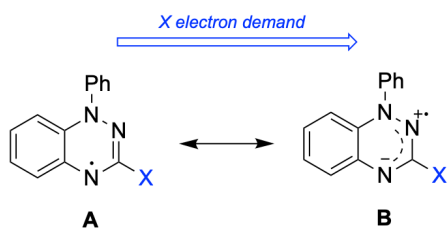
Scheme 27. Resonance structures of Blatter radicals based on observations made in Ref. [57].

The properties described can be rationalised from the basic topology of the SOMO, recently imaged by Kondo resonance mapping (Figure 12).[92] Since the orbital is predominately delocalised over the benzotriazine but possesses a node at C3, the result is the accumulation of very little spin density in the 3-substituent, such that its influence is largely a result of both spin polarization and the stability of the dipolar resonance contributor **B** (Scheme 27).[57] Kaszyński has discussed and correlated these substituent effects previously.[64]

3.3 Crystal Structures

The crystal structure of Blatter's radical and countless other species can be found on online databases.[93] In general, the amidrazonyl moiety adopts a planar or near-planar geometry with the fused arene, presumably driven by resonance stabilization of the unpaired electron. Aryl substituents at C3 are close to coplanar with the benzotriazine, whilst steric interactions between the peri hydrogen H(6) and the *ortho* position at N1 result in large torsional angles often greater than 50˚.

Figure 13. (*Left*) Geometry of Blatter's radical **9** in the crystalline phase. (*Right*) π-stacked chain of Blatter's radicals along the *b* crystallographic axis.[94]
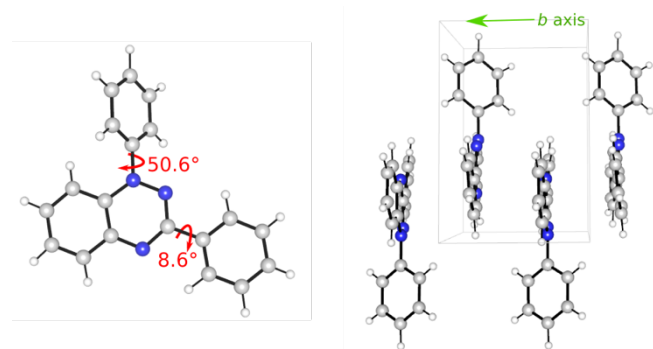
Blatter radicals crystallise as dark, typically red-black, prismatic needles. Most examples adopt a monoclinic symmetry similar to **9**, which occupies the P2₁/n space group,[94] however orthorhombic and triclinic examples have been reported. These arrangements describe slipped one-dimensional π-stacks of radicals, with short interplanar distances of 3–4 Å and high packing coefficients, typically to the exclusion of solvent. Interactions are primarily of face-to-face (π–π) but also edge-to-face (C-H···π) character, although the presence of bulky groups is known to preclude the aggregation of such π systems.[63,95]
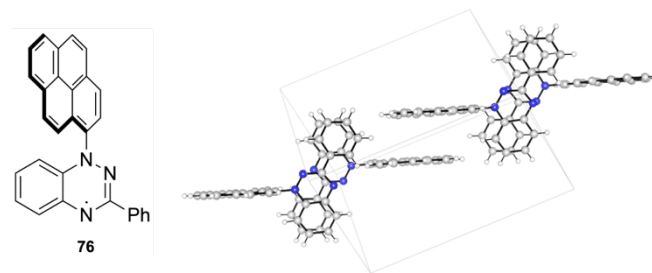
Figure 14. Packing excerpt of **76** showing one chain in the sheet of dimers propagating along the *ab* crystallographic plane.[96]

Many Blatter radicals form columns of dimers described by an inversion in the orientation of the N1 substituent along the stacking direction (see Figure 13). A veritable subset of these possess an additional symmetry element in the form of a centre of inversion, resulting in the appearance of two distinct centrosymmetric radical dimers. Recent studies by Kaszyński *et al.* have added new, more complex structures to the library, such as the 1-pyrenyl radical **76**, which forms sheets of double homo-co-facial π–π dimers (Figure 14).[96] These discoveries further realise the role of the N1 substituent,[97] particularly its steric demands, in dictating the packing arrangements characterising the polycrystalline phase.

3.4 Stability

Few focussed studies have been made on the specific decomposition pathways of Blatter radicals. Nevertheless, some general comments are possible with reference to the conditions under which they have been exposed. Like nitroxides, Blatter radicals rarely dimerise and are generally stable to molecular oxygen and water, hence the label of *stable*. Except for certain electron-rich examples, they are also unreactive to silica-gel chromatography and therefore purifiable using standard techniques.
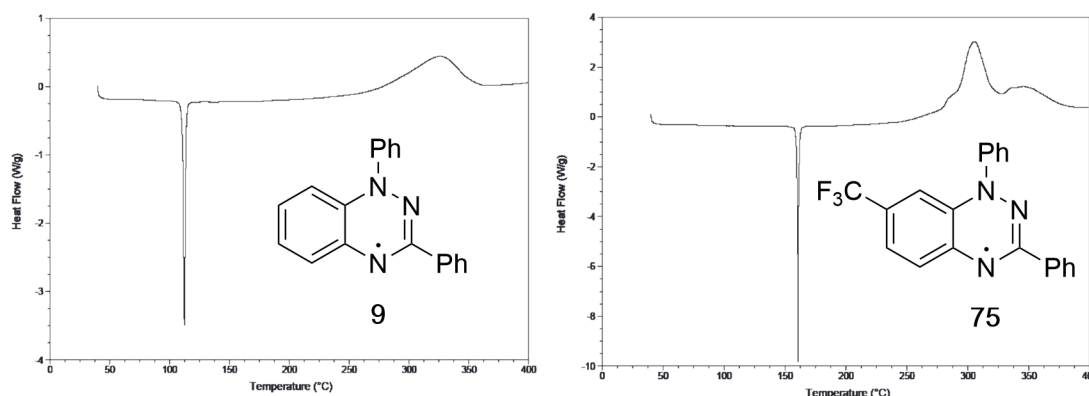
Figure 15. Differential scanning calorimetry trace of Blatter's radical **9** (*left*) and its 7-trifluoromethyl analogue **75** (*right*) from 40–400 °C at 5 °C/min under an Ar atmosphere. Reproduced with permission from Ref. [71]. Copyright (2011) American Chemical Society.

Blatter radicals exhibit exceptional thermal stability in the solid and the solution phases (Figure 15),[71] with decomposition onsets measured all the way up to 400 ˚C.[98] They are also excellent traps for carbon-centred radicals, exhibiting Gibbs free bond dissociation energies of the order of 100 kJ mol^{-1} or more at 298 K at the N4 position.[99,100] As seen in studies of controlled radical polymerization (Section 4.5), this trapping only becomes partially reversible above 100 °C.[101,102] Although there is a clear preference for radical coupling to N4, N2 regioisomers have been reported as far back as Neugebauer.[41,103] These species are less stable in general,[47] readily decomposing under heat or light exposure.

3.5 Redox Chemistry

Unlike the verdazyl or nitroxide radicals,[104,105] no dedicated study of basic Blatter electrochemistry has been added to the literature. This said, since it is common to perform voltammetric measurements in characterising new and existing species, abundant data has been produced over the years and the behaviour is well-understood.[45,49,64]
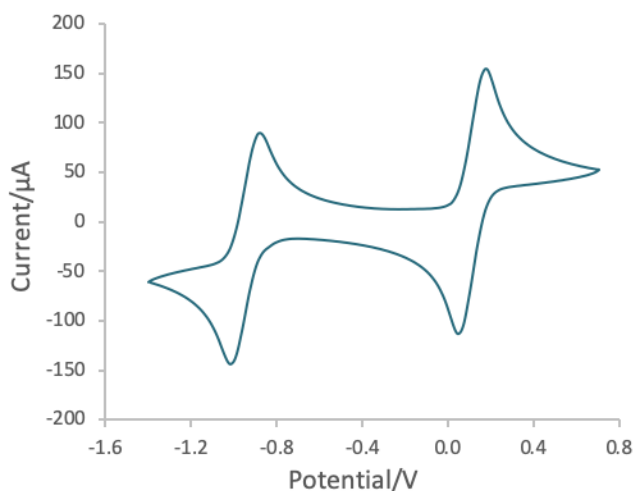
Figure 16. Cyclic voltammogram (100 mV s^{-1}) of **10** (100 µM) in MeCN and 0.1 M Bu$_4$NClO$_4$ with respect to Ag/AgCl at room temperature. Experimental details can be found in the Electronic Supplementary Information.

Blatter radicals undergo at least one reversible oxidation and one reversible reduction event (Figure 16). Consistent with Kaszyński's observation of the thioaminyl radicals,[106] these radicals being delocalised, exhibit narrow cell potentials ($E_{cell} = |E_{ox}° - E_{red}°|$) of around 1 V. Two unusual exceptions can be found in the 1,3-bis(pyrid-2-yl) radical **77** and the 3-(4-nitrophenyl) radical **78**, which endure two reversible oxidation and reduction events, respectively. The former case has been attributed to a spurious dimeric species (Figure 17),[107] whilst the latter corresponds to a follow-up reduction of NO$_2$, which, due to its disposition, does not directly participate in the initial reduction of the radical (*vide infra*).
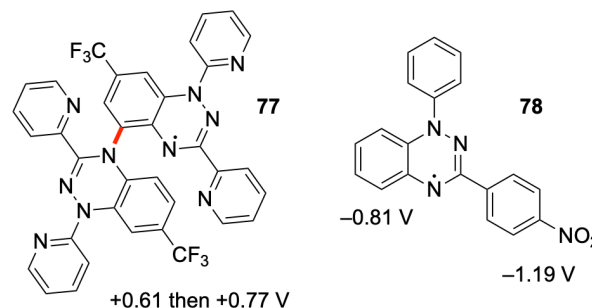
Figure 17. Most Blatter radicals exhibit one reversible oxidation and one reversible reduction event, one accidental and one real exception are illustrated here.[45,49,107]

The stability of the "12π" anion and the "10π" cation is highly sensitive to substituent effects, as is the radical. For example, Koutentis *et al.* tabulated a variation of 600 mV in the oxidation half-wave potentials and 360 mV in the reduction half-wave potentials across the various products of Scheme 19.[49] Typically, functionalisation of the C3 or C7 positions greatly influences both redox events as compared to Blatter's radical, whilst effective modification to the aromatic group at N1 is also known.[49] Interestingly, simultaneous functionalisation at C3 and C7 is considerably synergistic (Figure 18), revealing a structure that could play host to captodative effects by placing donor and acceptor groups at these opposing positions.[108]
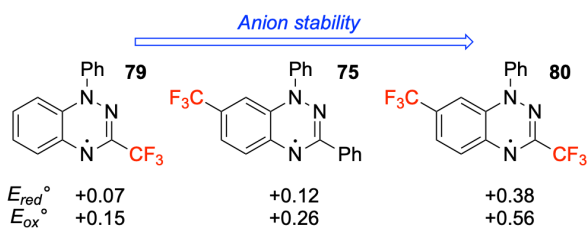
Figure 18. Redox properties of the trifluoromethylated radicals in CH_2Cl_2 vs Blatter's radical. Experimental details can be found in Ref. [45].

It is possible to correlate substituent effects with redox potentials by considering their respective Swain-Lupton *resonance* (R), and *field/inductive* (F) parameters.[109] Similar analyses with Hammett parameters have been performed previously.[64] To illustrate this case, Table 1 depicts this correlation for simple analogues of Blatter's radical in dichloromethane (Figure 19).

$R^1, R^3 = H, Me, OMe, NO_2, CF_3, Cl$
$R^2 = Ph, 4\text{-}(Me/OMe/NO_2/Cl)\text{-}C_6H_4$
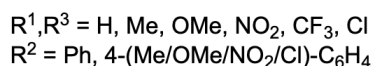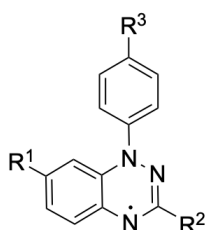
Figure 19. Substituent patterns considered in our correlation study.

For substituents at C7, considering either parameter in isolation yields no useful correlation ($R^2 < 0.75$), suggesting that the overall influence is a combination of the two. Indeed, scanning the ratio of R and F, excellent agreement ensues from mixed ratios of close to one-to-one. Similarly, a slight preference for F appears to be optimal at N1. This presumably stems from the high N1–Ar torsional angle with respect to the benzotriazine, which invariably reduces the opportunity for resonance stabilisation onto this group.

| Position		$x\mathbf{F} + y\mathbf{R}$	R^2	Slope
C7	$+e^-$	x = 0.5, y = 0.5	0.992	0.982
	$-e^-$	0.6, 0.4	0.977	0.982
C3	$+e^-$	0.1, 0.9	0.987	0.683
	$-e^-$	1.0, 0	0.958	0.870
N1	$+e^-$	0.6, 0.4	0.980	0.427
	$-e^-$	0.6, 0.4	0.975	0.930

Table 1. Linear regression modelling for reduction potentials of Blatter radicals against the modified Swain-Lupton parameters (R and F) of their respective substituent choices. Here we have constrained $x + y = 1$ with the accuracy of the resultant fit given by R^2. The importance of each position to the reduction potential is roughly accounted for by

the slope of the model, given in the right most column. All relevant data for this table can be found in the Electronic Supplementary Information.

Interestingly, whilst the reduction potential due to C3 is most closely correlated with the F parameter only, the oxidation potential is subject to both effects. This discrepancy is immediately resolved by appealing to the topology of the SOMO and ionic HOMO surfaces, depicted in figure 20. Clearly, the anionic HOMO and radical SOMO both share a node at C3, explaining the importance of the through-space interactions to reduction. Conversely, the cationic HOMO is delocalised into the substituent resulting in resonance stabilisation of the positive charge, hence a contribution from R.
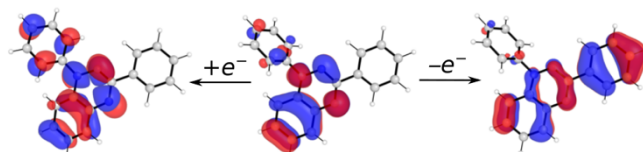
Figure 20. HOMO topology in Blatter's radical under electrochemical reduction (*Left*) and oxidation (*Right*).

4. Selected chemistry and applications

Owing to their extraordinary stability under ambient and exertive conditions, Blatter radicals have been considered in an ever-broadening variety of applications. These were discussed at length in Zheng's recent review which we revise briefly here.[38]

4.1 Sensors, Thin Films, Semiconductors and Spintronics

Historically, Blatter's radical was first reported as forming a pressure- sensitive charge transfer salt in combination with the electron acceptor, tetracyanoquinodimethane; these properties being fully reversible.[98,110] The pyrene-backed radical **81** is a known sensor for picric acid, which undergoes a stark colour change from purple to green (**82**) upon protonation in acetonitrile (Figure 21).[111] This species has also been closely examined for surface chemistry applications based on the high vapour pressure of pyrene. For example, highly air- and vacuum-stable magnetic thin films have been deposited on phosphorous-doped SiO_2 surfaces by organic molecular beam deposition,[112,113] whilst a copper-based surface was identified as a potential organic molecular quantum bit.[114]
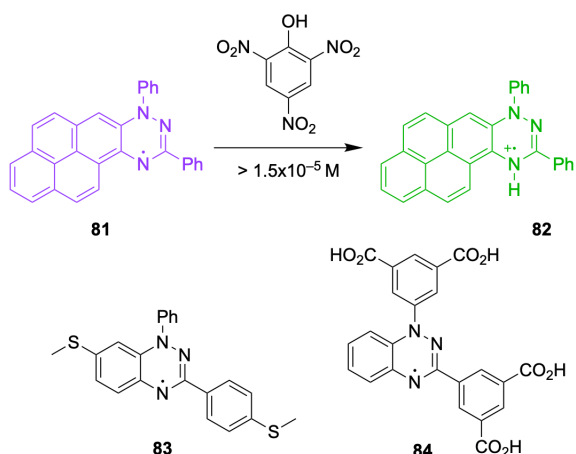
Figure 21. Functional analogues of Blatter's radical.[111,115,116]

Other functional modifications to Blatter's radical have since been reported, including the 3,7-dithiomethyl analogue **83**, synthesized for gold adhesion in single-molecule junctions[92,115] and the novel diamagnetic linker based on radical **84**.[116] This latter example was integrated into a copper based metal-organic framework (MOF) series, [Cu$_2$(TPTA)$_{1-x}$(**84**[-4H])$_x$], modulating its magnetic properties. Much like Kuhn-type verdazyl radicals,[117] Blatter radicals have also been identified for all-organic, rechargeable batteries,[118] where there is a palpable need for substrates possessing highly-stable oxidation states.[119,120] Currently unexplored is their capacity as spin-probes by flourence or EPR.[121] For example, oxoverdazyls and nitroxides are known to exhibit substituent-dependent profluorescence upon trapping of carbon-centred radicals.[122-124] We expect some scope for Blatter radicals in this respect.

4.2 Magnetic Materials

Stable organic radicals have long been studied as potential building blocks for molecule-based magnetic materials.[125,126] As with other applications, historically the literature has been more focused on nitroxide-based structures on account of their abundance and accessibility.[127,128] With the introduction of new gram-scale preparative methods, interest in Blatter-based magnetism has emerged from this trend. Readers will find a recent review by Mukhopadhyay et al. to be most useful on this topic.[39]
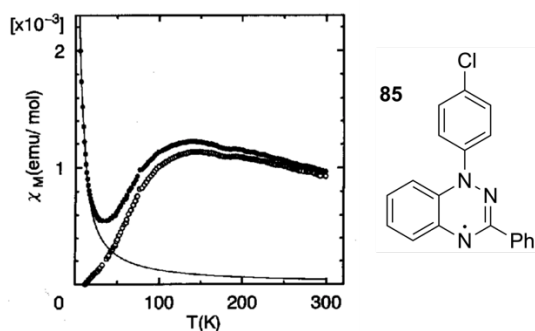
Figure 22. (Right) Temperature dependence of the molar magnetic susceptibility χ the 1-(4-chlorophenyl) radical **85**, with the solid line representing a (model) 3% radical impurity

curve and open circles revealing the difference. Reproduced with permission from Ref. [129]. Copyright (1994) Elsevier B.V.

In a pioneering report by Neugebauer et al., variable-temperature *magnetic susceptibility* (χ) measurements of Blatter's radical demonstrated typical Curie–Weiss behaviour over 7–300 K, with weak antiferromagnetic radical–radical coupling prevalent below 7 K.[129] Similar behaviour was observed in its 3-*tert*-butyl analogue **10** whilst the susceptibility of a 1-(4-chlorophenyl) species, **85** reached a broad maximum at 138 K, before rapidly descending due to the onset of notable short-range antiferromagnetism (Figure 22). In this case, a modified alternating, antiferromagnetic Heisenberg linear chain model proved a more appropriate fit.
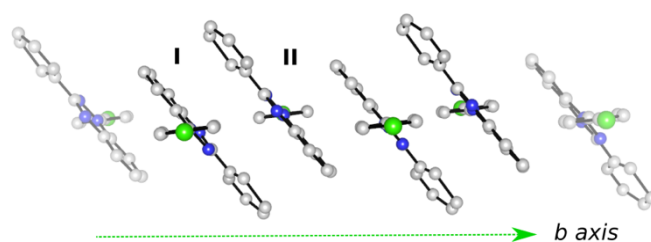
Figure 23. Crystal structure of **85** reduced to the *b* axis revealing the alternating sequence of centrosymmetric dimers, **I** and **II**.[129] Estimated exchange parameters of $J_1 = -76.5$ cm^{-1} and $J_2 = -22.9$ cm^{-1} were determined in Ref. [130].

Of course, the magnetic behaviour in the solid phase depends intimately on the crystal structure of the internal species (Section 3.3).[131,132] In the case of radicals **9** and **10**, the unpaired electrons are essentially encased between the mostly closed-shell C3 substituents of adjacent radicals in the π-stack (see Figure 13). This explains the incidence of paramagnetism up to ambient temperatures. By comparison, radical **85** forms chains of centrosymmetric dimers in which neighbouring benzotriazine moieties overlap (Figure 23). Such an arrangement welcomes the opportunity for exchange coupling interactions, hence a departure from simple Curie-Weiss behaviour.
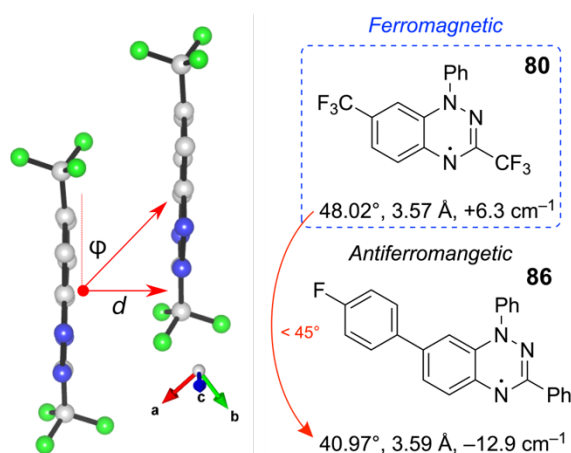
Figure 24: (*Left*) π-stacking in columns of radical **80**, where "*d*" is the shortest interplanar distance and "φ" is the *longitudinal* slippage angle, hydrogens removed for clarity.[133] (*Right*) Selected examples with respective geometric parameters *d*, φ and magnetic exchange interaction *J* are given beneath each figure.[134]

Due to the preference for columnar π-stacking in polycrystalline Blatter radicals, many examples are known to express unusual forms of low-dimensional magnetism.[135-137] For example, compounds such as the 3,7-bis(trifluoromethyl) radical **80**, which stack without N1–Ar inversion, tend to exhibit weak, long-range *intrachain* interactions but weaker (typically antiferromagnetic) *interchain* interactions. This results in essentially unidirectional magnetism of the form of a 1D Heisenberg linear chain (Figure 24).[133,134,138] The ultimate geometric and electronic factors governing the sign of the intrachain coupling is difficult to generalise however, but appears to involve the inter-planar separation as well as the slippage angles (principally the longitudinal) between successive radicals in the column. This in turn dictates the extent and character of the overlap between adjacent magnetic orbitals.[135] Of course, larger coupling constants are usually observed with small interplanar distances, the more subtle geometric feature being that large longitudinal slippage angles (>45°) can be characteristic of ferromagnetic (positive J) interactions,[111] antiferromagnetic (negative J) interactions *vice-versa*.[139,140]
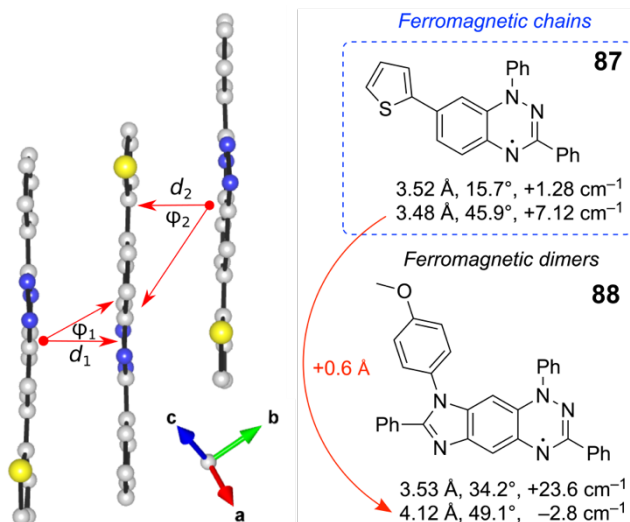

Figure 25. (*Left*) Dimeric stacking in columns of the 7-(thiophen-2-yl) radical (**87**) with hydrogens removed for clarity. (*Right*) Selected examples with relevant geometric parameters, *i.e.* $d_{1/2}$ and $\varphi_{1/2}$ between dimer 1 (*Top line*) and 2 (*Bottom line*) as well as the exchange parameters $J_{1/2}$ estimated from computional and magnetostructural modelling.[130,141]

The magnetic properties resulting from dimeric columns of Blatter radicals are more diverse and interesting due to the additional structural parameters.[87] Of course, due to the added structural complexities describing these morphologies, comparatively complex magneto-structural models must be fitted such that generalised statements become difficult.[63] These are usually low-dimensional in character however (Figure 25).[130,141]
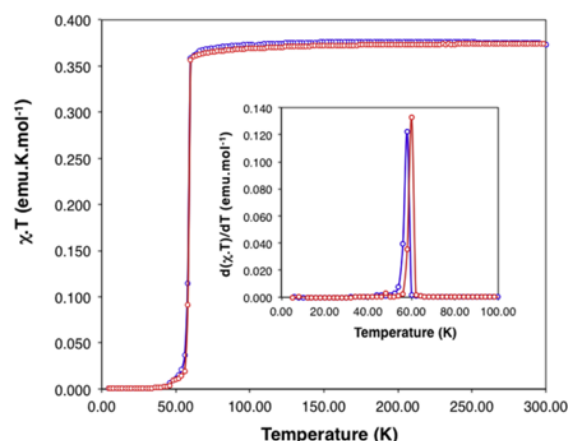

Figure 26. Variable temperature magnetic susceptibility χT of radical **79** upon cooling from 300 K (*Blue*) and heating from 5 K (*Red*). This transition involves an increase in the interplanar separations of 0.14 and 0.08 Å for d_1 and d_2, respectively (following conventions illustrated Figure 19), with changes in longitudinal slippage angles (φ_1 and φ_2) of +7.4 and −2.3 degrees, between 5 and 75 K.[46] Assuming a Bleaney-Bowers model for interacting pairs of half-integer spins,[142] this modest transformation results in a large increase in the predicted dimer exchange interaction J_1 (from a significant antiferromagnetic value of −184.8 cm^{-1} to a slight ferromagnetic value of +4.1 cm^{-1}) along with a minor increase in J_2 (from −8.3 to +7.0 cm^{-1}), resulting in essentially paramagnetic behaviour above 75 K. Reprinted with permission from Ref. [46]. Copyright (2014) American Chemical Society

Of particular note in the literature on Blatter magnetism is the 3-trifluoromethyl radical **79**.[46] Solids of this compound were found to exhibit a reversible and abrupt, first-order phase transition, from a low-temperature diamagnetic phase to a high-temperature paramagnetic phase at 58 K (Figure 26). Computational modelling supported a two-step dimeric mechanism, described by population of the triplet-excited state at $\sim T_{1/2}$, followed by modest structural relaxation of the triplet dimer.[143] Following this line of thinking, some effort has been made to develop a radical exhibiting this behaviour only at ambient temperatures or indeed, under alternate stimuli.[144]

4.4 Coordination complexes

The organometallic prospects of Blatter radicals are as usual, understudied by comparison to other species. Hexafluoroacetylacetone (hfac) complexes of divalent 3d transition-metals with the bipyridyl-like radical **90** were initially studied by Morgan and Koutentis *et al.* in the interest of developing metal–radical magnets.[145,146] Mn^{II}, Fe^{II}, Co^{II}, Cu^{II} and Ni^{II} species were prepared in a simple addition of the metal^{II}(hfac)$_2$ dihydrate to a stoichiometric quantity of **90** in chloroform at room temperature (Scheme 28). The resultant M(**90**)(hfac)$_2$ complexes could be purified by crystallization for yields of 30–60%, completing what is a simple but very adequate synthesis. It is worth noting here that the amidrazone precursor was prepared from a thioamide as opposed to the usual route through a hydrazonyl/imidoyl chloride (Scheme 10).
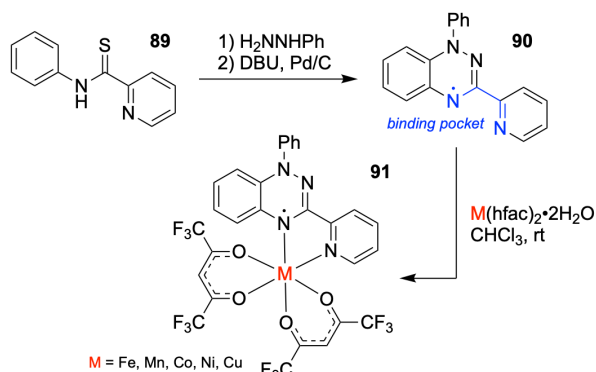
Scheme 28. Preparation of the metal-hfac complexes of 3-(pyrid-2-yl) radical **90**.[145,146]

Figure 28. (Left) Tetrahedral copper complex of **92**. (Right) Distorted triangular dodecahedron Dy[III] complex of **90** with H atoms and extraneous methyl groups removed.[149]

The binding mode of **90** was found to be bidentate in all species, resulting in pseudo-octahedral complexes of varying distortion. Magnetic-susceptibility measurements supported by computational modelling was carried out to determine their basic magnetic properties. To this end, the Mn[II] and Fe[II] complexes exhibited strong antiferromagnetic metal–radical coupling down to low cryogenic temperatures (< 30 K), whilst the Cu[II] and Ni[II] complexes behaved ferromagnetically in this respect. Radical–radical interactions were generally poor, particularly for Mn[II] and Fe[II], an observation rationalised by the limited opportunity for intermolecular SOMO–SOMO overlap apparent in their crystal structures (Figure 27). Non-negligible spin-orbit coupling prevented a similar deconvolution of the antiferromagnetic Co[II] complex, although a glance its structure would suggest similar traits.

Finally, the first lanthanide complex Dy(**90**)(tbacac)$_3$ (tbacac = 2,2,6,6-tetramethyl-3,5-heptanedionato) has been described by Morgan *et al.* as a case study for single-molecule magnets (Figure 28).[149,150] This compound, like the transition-metal species described above, is air and water stable, but by contrast, displays long-range, three-dimensional antiferromagnetism and slow relaxation mechanics. Computational considerations ruled out significant metal–radical and radical–radical interactions, leaving dipolar coupling between Dy[III] ions as the major factor behind its novel magnetic behavior.

4.4 Liquid Crystals

Among the more bespoke uses for Blatter radicals has been in the study of *liquid-crystalline* (LC) materials, recently reviewed by Kaszyński *et al.*, who has largely driven this work.[151] Following the latest preparative methods, Blatter radicals have been integrated into various mesogenic architectures, including discotic[152-154] and photoconductive bent-core structures[155,156] (Figure 29).

Figure 27. (*Left*) Distorted octahedral Mn[II] complex of **90**. (*Right*) Smallest asymmetric unit in the crystal structure of Ni(**90**)(hfac)$_2$ with H and F atoms removed for clarity.[145]

Recently, the first bis(triazinyl) metal salt, [Cu(**92**)$_2$](ClO$_4$)$_2$ · MeOH was reported (Figure 28).[147] This new tetrahedral complex exhibited all-round antiferromagnetic exchange interactions, whilst the hfac complex Cu(**92**)(hfac)$_2$, like its analogous complex of **90**, exhibited substantial ferromagnetic metal–radical coupling (J = +199 cm^{-1}). Zn[II], Ni[II] and Co[II] hfac complexes of **92** were later examined, however a transition metal complex exhibiting high-dimensional or long-range magnetic properties remains elusive.[148]

Half-disc

93: Ar = Ph

Disc

94: Ar = C_6H_2-3,4,5-$(SC_{12}H_{25})_3$

Bent-core

95: R^1 = $F(CF_2)_4(Ch_2)_6O$, R^2 = $F(CF_2)_6(CH_2)_8O$

Figure 29. Some mesogenic derivatives of Blatter radicals, figure adapted from Ref. [151].

In general, discotic mesogens adopt a columnar hexagonal phase below 80 ˚C, whilst bent-core mesogens form a Smectic A phase above 110 ˚C. The magnetic behaviour these phases is naturally controlled by this structuring and hence, the molecu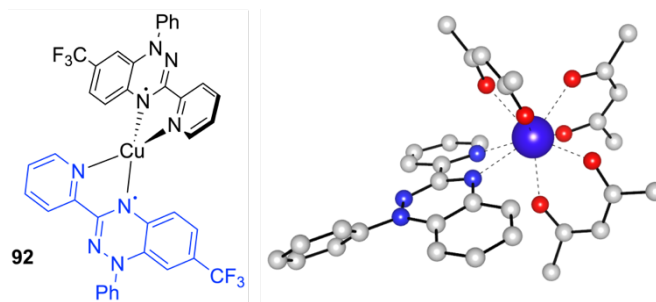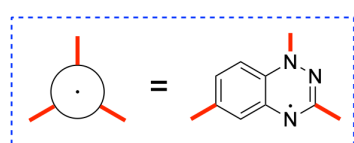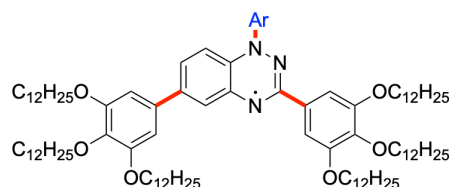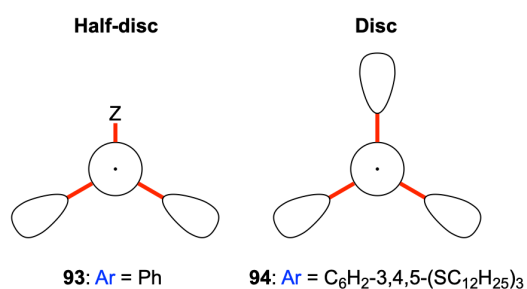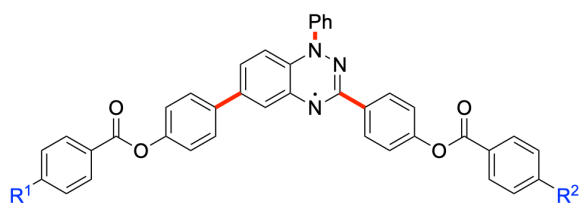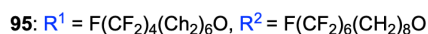lar geometry. For instance, half-disc mesogen **93** exhibits strong antiferromagnetic exchange interactions whereas the full-disc mesogen **94** is weakly ferromagnetic, with paramagnetic properties appearing at higher temperatures in the LC phase. Similarly, bent-core mesogen **95** forms nearly ideal paramagnets in the solid and LC phases, presumably due to steric barriers preventing SOMO–SOMO overlap thus isolating the radical centres.

4.5 High-Spin Molecular Systems

Some of the most compelling research in stable radical chemistry has been in the development di- and polyradicaloids.[157] These compounds, which possess thermally accessible spin states of use in magnetic materials and molecular electronics applications, have seen healthy progress in recent years, particularly now as the theory and design of such species has matured.[158-160]
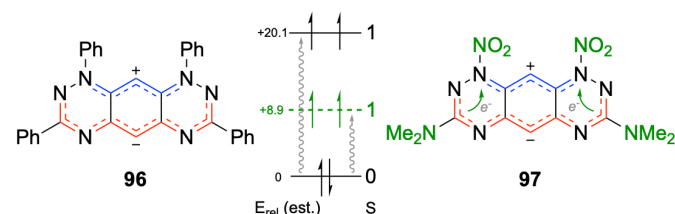
Figure 30. TPHA-1 (**96**) and its idealised "push-pull" adaption **97**, illustrating the effect on ΔE_{S-T} in kcal mol^{-1} (*Middle*). Details on the modelling can be found in Ref. [161].

The earliest compounds involving Blatter radical moieties were the *tetraphenylhexaazaanthracene's* (TPHA), of which so-called TPHA-1, **96** is the best-known example (Figure 30).[98,162,163] This benzo-fused analogue of Blatter's radical exists as an exceptionally stable zwitterion, defined by its large *singlet-triplet energy gap* (ΔE_{S-T}) of −20.1 kcal mol^{-1}. Redesigns and analogues of TPHA, such as **97**, have been proposed to reduce this veritable barrier,[161] however no example possessing a ground-state triplet have been realised thus far.[164]
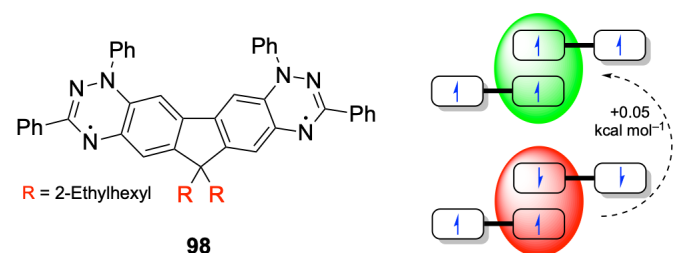
Figure 31. (*Left*) Diradicaloid **98** and (*Right*) cartoon representation of the intermolecular singlet (S = 0) and quintet (S = 2) dimer states.[165]

A large number of fused- and bridged-triazinyl polyradicals have also been reported over the years.[166-169] These compounds have numerous uses as discussed by Zheng *et al.*[38] Of particular note here is diradicaloid **98**, an excellent, near-infrared photodetector which exhibits doublet character in the solution phase but forms unusual, stable quintet dimers in the solid state.[165] Computational modelling revealed a small singlet-triplet gap (ΔE_{S-T} ~1.0 kcal mol^{-1}), leading the authors to posit that favourable exchange coupling in the dimer is responsible for a high-spin configuration accessible at room-temperature (Figure 31).[170] Further studies by the Zheng lab has extended the library of back-to-back bridged and fused Blatter diradicaloids, which now includes analogues of Chichibabin's **99** and Müller's hydrocarbons **100**,[171] as well as tetraphenylethylene-bridged (**101** and **102**) and nitrogen-bridged (**103** and **104**) species (Figure 32).[172,173] All of these examples exhibit an open-shell singlet ground state but a

thermally accessible triplet excited state. This apparent preference for antiferromagnetism in bridged diradicaloids now has computational precedence.[174]

99: n = 0
100: n = 1

ΔE_{S-T} = −1.05/1.27 kcal mol⁻¹

o-**101**: non-kekule
p-**102**: kekule

ΔE_{S-T} = −0.21/0.18 kcal mol⁻¹

R = 2-Ethylhexyl

103
104: Amiyl moiety

ΔE_{S-T} = −1.16/2.38 kcal mol⁻¹

Figure 32. Various Blatter diradicaloids examined by Zheng *et al*. (*Top*) Analogues of Chichibabin (n = 0) and Müller's (n = 1) hydrocarbons (high-lighted in blue).[171] (*Middle*) Tetraphenylethylene- and (*Bottom*) nitrogen-bridged Blatter diradicaloids.[172,173]

With the ultimate goal of developing an all-organic ferromagnet, polyradicals possessing a stable high-spin ground state are the most sought-after but rarest examples in the literature.[175] The Rajca group has prepared a handful of remarkable Blatter-based diradicals with stable triplet ground states, achieved through the attachment of an iminonitroxide or nitronyl nitroxide co-radical (Figure 33).[176] These diradicals are stable in air at room temperature, however examples of the robust nitronyl nitroxide moiety enjoy higher thermal decomposition onsets (> 160 ˚C under an inert atmosphere). The most recent addition **106**,[177] an evolution of **105**, has an ΔE_{S-T} of ≥ 1.7 kcal mol⁻¹, synonymous with 98% triplet occupancy at room temperature.

nitronyl nitroxide

0.50 kcal mol⁻¹
~85%

1.74 kcal mol⁻¹
~98%

105   **106**

oxoverdazyl

107

0.46 kcal mol⁻¹ (est.)
~84%
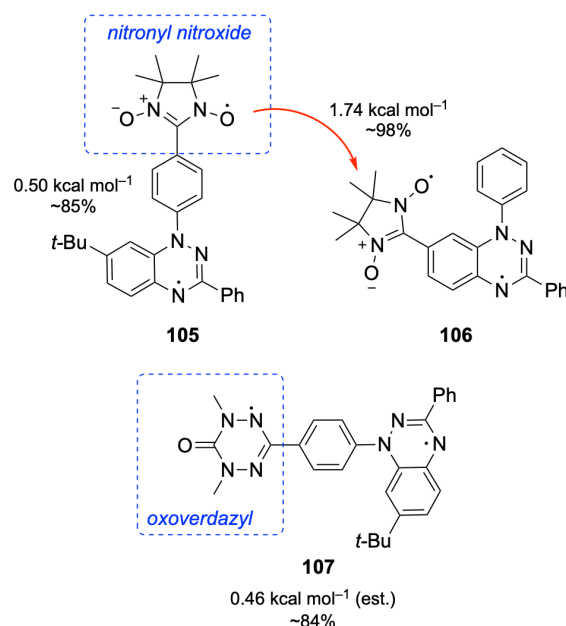
Figure 33. (*Top*) Heterogenous triplet diradicals based on the nitronyl nitroxide moiety studied by Rajca *et al*.[176,177] (*Bottom*) Proposed oxoverdazyl-bridged Blatter diradical modelled in Ref. [178]. ΔE_{S-T} and triplet occupancy given below each example.

The difficulty in designing high spin polyradicals is compounded by the often desire to establish long-range interactions in polycrystalline solids and films. Here, **106** is unusual in so far that is forms antiferromagnetic one-dimensional chains in th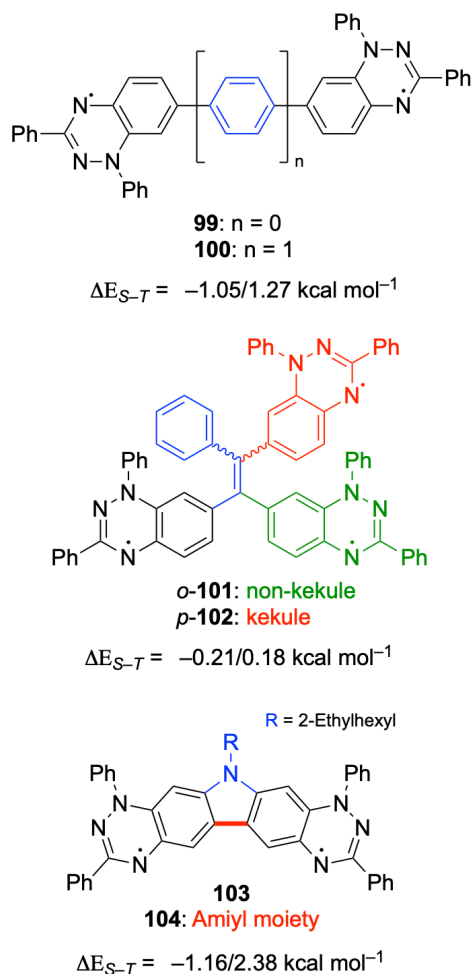e polycrystalline phase, with a coupling constant of J'/k = −14 K being "by far strongest among all studied 1D S = 1 chains of organic radicals". Some work is also required to develop the theory and preparation of air-stable, triplet diradicals suitable for device fabrication, for example, by evaporative methods. Currently, **105** and **106** are the only known examples which have been thermally sublimed under ultra-high vacuum with near full retention of diradical character. Rigorous calculations on a series of analogous diradicaloids has pointed to compounds based on for example, an air-stable oxoverdazyl **107**, which may well satisfy these needs.[178]

4.5 Synthetic Applications

Much like nitroxides and verdazyls, Blatter radicals are excellent traps for carbon-centred radicals and, due to their high radical stability, this trapping becomes partially reversible at high temperatures (*ca.* > 100 °C). As a result, Blatter radicals could in principle be harnessed to control radical polymerization by limiting the concentration of carbon-centred propagating radicals, relative to the number of dormant trapped species. In this way radical–radical termination can be minimised with respect to chain growth (Figure 34). Two studies interested in the capacity of Blatter radicals as mediators for controlled radical polymerization have been reported. Initial attempts to thermally polymerise styrene in the presence of Blatter's radical and select analogues were generally successful, with reasonable control achieved at 125 °C (polydispersity 1.2 for molecular weights up to 14 kg mol⁻¹).[101] High control was also observed in the polymerization of various styrenic and acrylate

(co)polymers with unimolecular Blatter-initiators,[102] however no improvement over conventional nitroxide-based mediators has been demonstrated thus far. This said, the inherent tunability of Blatter radicals may well come as an advantage in more bespoke photo- and electro-induced polymerizations, both of which have curried great interest in recent literature.[179-183]

Figure 34. Control equilibrium in Blatter-mediated radical polymerization, illustrated using Blatter's radical as the control agent for a generic polymer P_N.

Another possible synthetic application of the carbon-centred radical-adducts of Blatter radicals is in oxidative cleavage. As context, theoretical and experimental studies have shown that TEMPO-based alkoxyamines can undergo oxidative cleavage to either nitroxide radicals and carbocations, or oxoammonium ca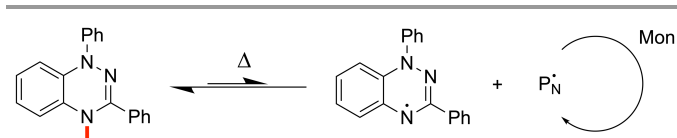tions and carbon-centred radicals, according to the stability of the leaving carbocation or carbon-centred radical.[184-186] When the leaving group is not stable in either form, the oxidation is reversible unless a nucleophile is present, in which case cleavage is driven by an S_N2 process.[187] This chemistry can be used to afford *in situ* methylation with high yield and broad scope.[188] Although experiments have yet to be reported, high-level theoretical calculations have shown that Blatter radicals also undergo oxidative cleavage, and because they undergo oxidation at considerably lower potentials than alkoxyamines, they offer the opportunity to broaden the functional group tolerance of this chemistry (Figure 35).[99,189]
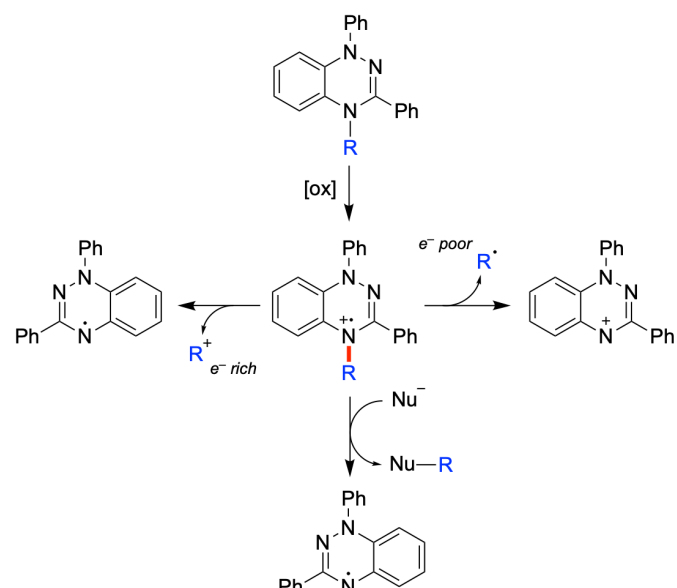
Figure 35. Behaviour of Blatter radical adducts under oxidation and their potential applications as radical sources, carbocations and methylating agents.[99,189]

Conclusions

Previously an object of curiosity, Blatter radicals have enjoyed vigorous development over this last decade. Several new synthetic strategies, at least three of which are generally applicable, have been added to the literature, with numerous options for derivatisation also being demonstrated. These tools, along with new computational insights, has opened the door to the new frontiers of rational design, leading to the preparation of numerous "tailor-made" compounds which meet the needs of the latest technologies in materials chemistry. Already, Blatter radicals are finding applications in magnetic materials, as sensors, spin labels and liquid crystals. They have even been proposed as potential qubits in quantum computing and have developing applications in polymer and small molecule synthesis. With their high stability, ease of preparation and functionalisation, diverse and tuneable properties, their use in functional materials is set to expand.

Conflicts of interest

There are no conflicts to declare.

Acknowledgements

Notes and references

1. D. Griller and K. U. Ingold, *Acc. Chem. Res.*, 1976, **9**, 13-19.
2. R. G. Hicks, *Org. Biomol. Chem.*, 2007, **5**, 1321-1338.
3. M. Gomberg, *J. Am. Chem. Soc.*, 1900, **22**, 757-771.
4. R. I. Walter, *J. Am. Chem. Soc.*, 1955, **77**, 5999-6002.
5. F. A. Bell, A. Ledwith and D. C. Sherrington, *J. Chem. Soc. C*, 1969, 2719-2720.
6. D. J. Bellville, D. W. Wirth and N. L. Bauld, *J. Am. Chem. Soc.*, 1981, **103**, 718-720.
7. J. P. Barham, M. P. John and J. A. Murphy, *J. Am. Chem. Soc.*, 2016, **138**, 15482-15487.
8. J. Petkus and K. Shubin, *Chem. Heterocycl. Compd.*, 2020, **56**, 512-514.
9. M. Kuratsu, M. Kozaki and K. Okada, *Angew. Chem.*, 2005, **44**, 4056-4058.
10. T. A. Schaub, T. Mekelburg, P. O. Dral, M. Miehlich, F. Hampel, K. Meyer and M. Kivala, *Chem. Eur. J.*, 2020, **26**, 3264-3269.
11. A. Nilsen and R. Braslau, *J. Polym. Sci. A Polym. Chem.*, 2006, **44**, 697-717.
12. D. Bardelang, M. Hardy, O. Ouari and P. Tordo, in *Encyclopedia of Radicals in Chemistry, Biology and Materials*, John Wiley & Sons, New Jersey, 2012, vol. 3.
13. D. Goldfarb and S. Stoll, *EPR spectroscopy: fundamentals and methods*, John Wiley & Sons, 2018.
14. L. Buzzetti, G. E. M. Crisenza and P. Melchiorre, *Angew. Chem.*, 2019, **58**, 3730-3747.

15. K. U. Ingold and D. A. Pratt, *Chem. Rev.*, 2014, **114**, 9022-9046.
16. J. M. Hoover and S. S. Stahl, *J. Am. Chem. Soc.*, 2011, **133**, 16901-16910.
17. S. Wertz and A. Studer, *Green Chem.*, 2013, **15**, 3116-3134.
18. C. J. Hawker, A. W. Bosman and E. Harth, *Chem. Rev.*, 2001, **101**, 3661-3688.
19. J. Nicolas, Y. Guillaneuf, C. Lefay, D. Bertin, D. Gigmes and B. Charleux, *Prog. Polym. Sci.*, 2013, **38**, 63-235.
20. G. Gryn'ova, L. M. Smith and M. L. Coote, *Phys. Chem. Chem. Phys.*, 2017, **19**, 22678-22683.
21. T. Janoschka, M. D. Hager and U. S. Schubert, *Adv. Mater.*, 2012, **24**, 6397-6409.
22. S. Muench, A. Wild, C. Friebe, B. Häupler, T. Janoschka and U. S. Schubert, *Chem. Rev.*, 2016, **116**, 9438-9484.
23. L. Tebben and A. Studer, *Angew. Chem.*, 2011, **50**, 5034-5068.
24. G. Gryn'ova, J. M. Barakat, J. P. Blinco, S. E. Bottle and M. L. Coote, *Chem. Eur. J.*, 2012, **18**, 7582-7593.
25. K. Zhang, B. B. Noble, A. C. Mater, M. J. Monteiro, M. L. Coote and Z. Jia, *Phys. Chem. Chem. Phys.*, 2018, **20**, 2606-2614.
26. M. Lewandowski and K. Gwozdzinski, *Int. j. mol. sci.*, 2017, **18**, 2490.
27. B. P. Soule, F. Hyodo, K.-I. Matsumoto, N. L. Simone, J. A. Cook, M. C. Krishna and J. B. Mitchell, *Free rad. biol. med.*, 2007, **42**, 1632-1650.
28. K.-A. Hansen and J. P. Blinco, *Polym. Chem.*, 2018, **9**, 1479-1516.
29. R. Kuhn and H. Trischmann, *Angew. Chem.*, 1963, **2**, 155-155.
30. R. Kuhn and H. Trischmann, *Monatsh. Chem.*, 1964, **95**, 457-479.
31. F. A. Neugebauer, *Angew. Chem.*, 1973, **12**, 455-464.
32. F. A. Neugebauer, H. Fischer and R. Siegel, *Chem. Ber.*, 1988, **121**, 815-822.
33. O. M. Polumbrik, *Russ. Chem. Rev.*, 1978, **47**, 767-785.
34. B. D. Koivisto and R. G. Hicks, *Coord. Chem. Rev.*, 2005, **249**, 2612-2630.
35. G. N. Lipunova, T. G. Fedorchenko and O. N. Chupakhin, *Russ. Chem. Rev.*, 2013, **82**, 701-734.
36. J. B. Gilroy, PhD Thesis, 2008.
37. C. P. Constantinides and P. A. Koutentis, in *Advances in Heterocyclic Chemistry*, eds. E. F. V. Scriven and C. A. Ramsden, Academic Press, 2016, vol. 119, pp. 173-207.
38. Y. Ji, L. Long and Y. Zheng, *Mater. Chem. Front.*, 2020, DOI: 10.1039/D0QM00122H.
39. S. Kumar, Y. Kumar, S. K. Keshri and P. Mukhopadhyay, *Magnetochemistry*, 2016, **2**, 42.
40. H. M. Blatter and H. Lukaszewski, *Tetrahedron Lett.*, 1968, **9**, 2701-2705.
41. F. A. Neugebauer and I. Umminger, *Chem. Ber.*, 1980, **113**, 1205-1225.
42. F. A. Neugebauer and I. Umminger, *Chem. Ber.*, 1981, **114**, 2423-2430.
43. F. A. Neugebauer and G. Rimmler, *Magn. Reson. Chem.*, 1988, **26**, 595-600.
44. P. A. Koutentis and D. Lo Re, *Synthesis*, 2010, **2010**, 2075-2079.
45. A. A. Berezin, G. Zissimou, C. P. Constantinides, Y. Beldjoudi, J. M. Rawson and P. A. Koutentis, *J. Org. Chem.*, 2014, **79**, 314-327.
46. C. P. Constantinides, A. A. Berezin, G. A. Zissimou, M. Manoli, G. M. Leitus, M. Bendikov, M. R. Probert, J. M. Rawson and P. A. Koutentis, *J. Am. Chem. Soc.*, 2014, **136**, 11906-11909.
47. C. P. Constantinides, E. Obijalska and P. Kaszyński, *Org. Lett.*, 2016, **18**, 916-919.
48. J. A. Grant, Z. Lu, D. E. Tucker, B. M. Hockin, D. S. Yufit, M. A. Fox, R. Kataky, V. Chechik and A. C. O'Donoghue, *Nat. Commun.*, 2017, **8**, 15088.
49. A. C. Savva, S. I. Mirallai, G. A. Zissimou, A. A. Berezin, M. Demetriades, A. Kourtellaris, C. P. Constantinides, C. Nicolaides, T. Trypiniotis and P. A. Koutentis, *J. Org. Chem.*, 2017, **82**, 7564-7575.
50. M. Busch and R. Ruppenthal, *Chem. Ber.*, 1910, **43**, 3001-3011.
51. R. Huisgen and J. Wulff, *Chem. Ber.*, 1969, **102**, 1848-1858.
52. T. L. Gilchrist, C. J. Harris and C. W. Rees, *Chem. Commun.*, 1974, 485-486.
53. D. H. R. Barton, J. W. Ducker, W. A. Lord and P. D. Magnus, *Perkin Trans. 1*, 1976, 38-42.
54. B. I. Buzykin and N. G. Gazetdinova, *Bull. Russ. Acad. Sci.: Chem.*, 1980, **29**, 1159-1163.
55. R. Fusco and F. Sannicolo, *Tetrahedron Lett.*, 1982, **23**, 1829-1830.
56. R. Fusco, A. Marchesini and F. Sannicolò, *J. Heterocycl. Chem.*, 1986, **23**, 1795-1799.
57. A. Bodzioch, M. Zheng, P. Kaszyński and G. Utecht, *J. Org. Chem.*, 2014, **79**, 7294-7310.
58. W. Hou, N. A. Dehm and R. W. J. Scott, *J. Catal.*, 2008, **253**, 22-27.
59. T. Mallat and A. Baiker, *Catal. Today*, 1994, **19**, 247-283.
60. G.-J. t. Brink, I. W. C. E. Arends and R. A. Sheldon, *Science*, 2000, **287**, 1636.
61. X. Xiong, Y. Jiang and D. Ma, *Org. Lett.*, 2012, **14**, 2552-2555.
62. K. Fukui, T. Yonezawa and H. Shingu, *J. Chem. Phys.*, 1952, **20**, 722-725.
63. F. Bazzi, A. J. Danke, D. B. Lawson, M. Manoli, G. M. Leitus, P. A. Koutentis and C. P. Constantinides, *CrystEngComm*, 2020, **22**, 4306-4316.
64. D. Pomikło, A. Bodzioch, A. Pietrzak and P. Kaszyński, *Org. Lett.*, 2019, **21**, 6995-6999.
65. A. Bodzioch, D. Pomikło, M. Celeda, A. Pietrzak and P. Kaszyński, *J. Org. Chem.*, 2019, **84**, 6377-6394.
66. P. Kaszyński, C. P. Constantinides and V. G. Young Jr, *Angew. Chem.*, 2016, **55**, 11149-11152.
67. P. Bartos, B. Anand, A. Pietrzak and P. Kaszyński, *Org. Lett.*, 2020, **22**, 180-184.
68. P. Bartos, V. G. Young and P. Kaszyński, *Org. Lett.*, 2020, DOI: 10.1021/acs.orglett.0c01074.
69. M. Catto, A. A. Berezin, D. Lo Re, G. Loizou, M. Demetriades, A. De Stradis, F. Campagna, P. A. Koutentis and A. Carotti, *Eur. J. Med. Chem.*, 2012, **58**, 84-97.
70. M. Sweeney, R. Coyle, P. Kavanagh, A. A. Berezin, D. Lo Re, G. A. Zissimou, P. A. Koutentis, M. P. Carty and F. Aldabbagh, *Bioorg. Med. Chem.*, 2016, **24**, 3565-3570.

71. C. P. Constantinides, P. A. Koutentis, H. Krassos, J. M. Rawson and A. J. Tasioupoulos, *J. Org. Chem.*, 2011, **76**, 2798-2806.

72. C. P. Constantinides, P. A. Koutentis and G. Loizou, *Org. Biomol. Chem.*, 2011, **9**, 3122-3125.

73. L.-A. J. Keane, S. I. Mirallai, M. Sweeney, M. P. Carty, G. A. Zissimou, A. A. Berezin, P. A. Koutentis and F. Aldabbagh, *Molecules*, 2018, **23**, 574.

74. G. A. Zissimou, A. Kourtellaris, M. Manoli and P. A. Koutentis, *J. Org. Chem.*, 2018, **83**, 9391-9402.

75. A. A. Berezin, C. P. Constantinides, C. Drouza, M. Manoli and P. A. Koutentis, *Org. Lett.*, 2012, **14**, 5586-5589.

76. A. A. Berezin, C. P. Constantinides, S. I. Mirallai, M. Manoli, L. L. Cao, J. M. Rawson and P. A. Koutentis, *Org. Biomol. Chem.*, 2013, **11**, 6780-6795.

77. A. A. Berezin and P. A. Koutentis, *Org. Biomol. Chem.*, 2014, **12**, 1641-1648.

78. D. Zhao, J. Hu, N. Wu, X. Huang, X. Qin, J. Lan and J. You, *Org. Lett.*, 2011, **13**, 6516-6519.

79. P. Thapa, P. M. Palacios, T. Tran, B. S. Pierce and F. W. Foss, *J. Org. Chem.*, 2020, **85**, 1991-2009.

80. F. M. Romero and R. Ziessel, *Tetrahedron Lett.*, 1999, **40**, 1895-1898.

81. C. Stroh, M. Mayor and C. von Hänisch, *Eur. J. Org. Chem.*, 2005, **2005**, 3697-3703.

82. C. Stroh, M. Mayor and C. v. Hänisch, *Tetrahedron Lett.*, 2004, **45**, 9623-9626.

83. C. P. Constantinides, P. A. Koutentis and G. Loizou, *Organic & Biomolecular Chemistry*, 2011, **9**, 3122-3125.

84. T.-N. Le, T. Trevisan, E. Lieu and D. J. R. Brook, *Eur. J. Org. Chem.*, 2017, **2017**, 1125-1131.

85. P. V. Petunin, D. E. Votkina, M. E. Trusova, T. V. Rybalova, E. V. Amosov, M. N. Uvarov, P. S. Postnikov, M. S. Kazantsev and E. A. Mostovich, *New J. Chem.*, 2019, **43**, 15293-15301.

86. Y. Takahashi, Y. Miura and N. Yoshioka, *Chem. Lett.*, 2014, **43**, 1236-1238.

87. C. P. Constantinides, E. Carter, D. M. Murphy, M. Manoli, G. M. Leitus, M. Bendikov, J. M. Rawson and P. A. Koutentis, *Chem. Commun.*, 2013, **49**, 8662-8664.

88. G. Karecla, P. Papagiorgis, N. Panagi, G. A. Zissimou, C. P. Constantinides, P. A. Koutentis, G. Itskos and S. C. Hayes, *New J. Chem.*, 2017, **41**, 8604-8613.

89. J. Kido, M. Kimura and K. Nagai, *Science*, 1995, **267**, 1332.

90. M. K. Kadirov, A. V. Il'yasov, A. A. Vafina, B. I. Buzykin, N. G. Gazetdinova and Y. P. Kitaev, *Bull. Russ. Acad. Sci.: Chem.*, 1984, **33**, 649-650.

91. M. K. Kadirov, B. I. Buzykin and N. G. Gazetdinova, *Russ. Chem. Bull.*, 2002, **51**, 1796-1799.

92. L. L. Patera, S. Sokolov, J. Z. Low, L. M. Campos, L. Venkataraman and J. Repp, *Angew. Chem.*, 2019, **58**, 11063-11067.

93. C. R. Groom, I. J. Bruno, M. P. Lightfoot and S. C. Ward, *Acta. Crystallogr. B. Struct. Sci.*, 2016, **72**, 171-179.

94. A. T. Gubaidullin, B. I. Buzykin, I. A. Litvinov and N. G. Gazetdinova, *Russ. J. Chem.*, 2004, **74**, 939-943.

95. C. Constantinides, A. Berezin, G. Zissimou, M. Manoli, G. Leitus and P. Koutentis, *Molecules*, 2016, **21**, 636.

96. A. Gardias, P. Kaszyński, E. Obijalska, D. Trzybiński, S. Domagała, K. Woźniak and J. Szczytko, *Chem. Eur. J.*, 2018, **24**, 1317-1329.

97. C. P. Constantinides, D. B. Lawson, G. A. Zissimou, A. A. Berezin, A. Mailman, M. Manoli, A. Kourtellaris, G. M. Leitus, R. Clérac, H. M. Tuononen and P. A. Koutentis, *CrystEngComm*, 2020, DOI: 10.1039/D0CE00789G.

98. K. A. Hutchison, Ph.D., University of California, Santa Barbara, 1998.

99. F. J. M. Rogers and M. L. Coote, *J. Phys. Chem. C*, 2019, **123**, 10306-10310.

100. F. J. M. Rogers and M. L. Coote, *J. Phys. Chem. C*, 2019, **123**, 20174-20180.

101. M. Demetriou, A. A. Berezin, P. A. Koutentis and T. Krasia-Christoforou, *Polym. Int.*, 2014, **63**, 674-679.

102. J. Areephong, K. M. Mattson, N. J. Treat, S. O. Poelma, J. W. Kramer, H. A. Sprafke, A. A. Latimer, J. Read de Alaniz and C. J. Hawker, *Polym. Chem.*, 2016, **7**, 370-374.

103. P. Kaszyński, A. Kłys, S. Domagała and K. Woźniak, *Tetrahedron*, 2017, **73**, 3823-3830.

104. J. B. Gilroy, S. D. J. McKinnon, B. D. Koivisto and R. G. Hicks, *Org. Lett.*, 2007, **9**, 4837-4840.

105. J. P. Blinco, J. L. Hodgson, B. J. Morrow, J. R. Walker, G. D. Will, M. L. Coote and S. E. Bottle, *J. Org. Chem.*, 2008, **73**, 6763-6771.

106. P. Kaszynski, *J. Phys. Chem. A*, 2001, **105**, 7626-7633.

107. A. A. Berezin, G. Zissimou, C. P. Constantinides, Y. Beldjoudi, J. M. Rawson and P. A. Koutentis, *J. Org. Chem.*, 2015, **80**, 8943-8944.

108. H. G. Viehe, Z. Janousek, R. Merenyi and L. Stella, *Acc. Chem. Res.*, 1985, **18**, 148-154.

109. C. G. Swain and E. C. Lupton, *J. Am. Chem. Soc.*, 1968, **90**, 4328-4337.

110. K. Hutchison, G. Srdanov, R. Menon, J.-C. Gabriel, B. Knight and F. Wudl, *Synth. Met.*, 1997, **86**, 2147-2148.

111. Y. Zheng, M.-s. Miao, M. C. Kemei, R. Seshadri and F. Wudl, *Isr. J. Chem.*, 2014, **54**, 774-778.

112. F. Ciccullo, N. M. Gallagher, O. Geladari, T. Chassé, A. Rajca and M. B. Casu, *ACS Appl. Mater. Int.*, 2016, **8**, 1805-1812.

113. M. B. Casu, *Acc. Chem. Res.*, 2018, **51**, 753-760.

114. F. Ciccullo, A. Calzolari, K. Bader, P. Neugebauer, N. M. Gallagher, A. Rajca, J. van Slageren and M. B. Casu, *ACS Appl. Mater. Int.*, 2019, **11**, 1571-1578.

115. J. Z. Low, G. Kladnik, L. L. Patera, S. Sokolov, G. Lovat, E. Kumarasamy, J. Repp, L. M. Campos, D. Cvetko, A. Morgante and L. Venkataraman, *Nano Letters*, 2019, **19**, 2543-2548.

116. A. S. Poryvaev, D. M. Polyukhov, E. Gjuzi, F. Hoffmann, M. Fröba and M. V. Fedin, *Inorg. Chem.*, 2019, **58**, 8471-8479.

117. G. D. Charlton, S. M. Barbon, J. B. Gilroy and C. A. Dyker, *J. Energ. Chem.*, 2019, **34**, 52-56.

118. B. Häupler, U. S. Schubert, A. Wild, P. A. Koutentis and G. Zissimou, *German Patent*, 2018, DE102017005924.

119. C. Friebe and U. S. Schubert, *Top. Curr. Chem.*, 2017, **375**, 65-99.

120. C. Friebe, A. Lex-Balducci and U. S. Schubert, *ChemSusChem*, 2019, **12**, 4093-4115.

121. A. Kaur, J. L. Kolanowski and E. J. New, *Angew. Chem.*, 2016, **55**, 1602-1613.

122. D. Matuschek, S. Eusterwiemann, L. Stegemann, C. Doerenkamp, B. Wibbeling, C. G. Daniliuc, N. L. Doltsinis, C. A. Strassert, H. Eckert and A. Studer, *Chem. Sci.*, 2015, **6**, 4712-4716.

123. S. Eusterwiemann, D. Matuschek, L. Stegemann, S. Klabunde, C. C. Doerenkamp, C. G. Daniliuc, N. L. Doltsinis, C. A. Strassert, H. Eckert and A. Studer, *CHIMIA*, 2016, **70**, 172-176.

124. J. P. Blinco, K. E. Fairfull-Smith, B. J. Morrow and S. E. Bottle, *Aust. J. Chem.*, 2011, **64**, 373-389.

125. I. Ratera and J. Veciana, *Chem. Soc. Rev.*, 2012, **41**, 303-349.

126. J. S. Miller, *Mater. Today*, 2014, **17**, 224-235.

127. C. Train, L. Norel and M. Baumgarten, *Coord. Chem. Rev.*, 2009, **253**, 2342-2351.

128. E. V. Tretyakov and V. I. Ovcharenko, *Russ. Chem. Rev.*, 2009, **78**, 971-1012.

129. K. Mukai, K. Inoue, N. Achiwa, J. B. Jamali, C. Krieger and F. A. Neugebauer, *Chem. Phys. Lett.*, 1994, **224**, 569-575.

130. C. P. Constantinides, P. A. Koutentis and J. M. Rawson, *Chem. Eur. J.*, 2012, **18**, 7109-7116.

131. Y. Miura and N. Yoshioka, *Chem. Phys. Lett.*, 2015, **626**, 11-14.

132. M. Fumanal, S. Vela, J. Ribas-Ariño and J. J. Novoa, *Chem. Asian J.*, 2014, **9**, 3612-3622.

133. C. P. Constantinides, D. B. Lawson, A. A. Berezin, G. A. Zissimou, M. Manoli, G. M. Leitus and P. A. Koutentis, *CrystEngComm*, 2019, **21**, 4599-4606.

134. C. P. Constantinides, P. A. Koutentis and J. M. Rawson, *Chem. Eur. J.*, 2012, **18**, 15433-15438.

135. J. P. Malrieu, R. Caballol, C. J. Calzado, C. de Graaf and N. Guihéry, *Chem. Rev.*, 2014, **114**, 429-492.

136. E. Coronado, *Nat. Rev. Mater.*, 2020, **5**, 87-104.

137. H. Mikeska and A. Kolezhuk, in *Quantum Magnetism. Lecture Notes in Physics*, eds. U. Schollwöck, J. Richter, D. J. J. Farnell and R. F. Bishop, Springer, Berlin, Heidelberg, 2004, vol. 645, pp. 1-83.

138. B. Yan, J. Cramen, R. McDonald and N. L. Frank, *Chem. Commun.*, 2011, **47**, 3201-3203.

139. C. P. Constantinides, A. A. Berezin, M. Manoli, G. M. Leitus, M. Bendikov, J. M. Rawson and P. A. Koutentis, *New J. Chem.*, 2014, **38**, 949-954.

140. Y. Takahashi, Y. Miura and N. Yoshioka, *New J. Chem.*, 2015, **39**, 4783-4789.

141. C. P. Constantinides, A. A. Berezin, M. Manoli, G. M. Leitus, G. A. Zissimou, M. Bendikov, J. M. Rawson and P. A. Koutentis, *Chem. Eur. J.*, 2014, **20**, 5388-5396.

142. B. Bleaney and K. Bowers, *Proc. Royal Soc. A*, 1952, **214**, 451-465.

143. M. Fumanal, S. Vela, J. J. Novoa and J. Ribas-Arino, *Chem. Commun.*, 2015, **51**, 15776-15779.

144. Y. Takahashi, N. Tsuchiya, Y. Miura and N. Yoshioka, *New J. Chem.*, 2018, **42**, 9949-9955.

145. I. S. Morgan, A. Mansikkamäki, G. A. Zissimou, P. A. Koutentis, M. Rouzières, R. Clérac and H. M. Tuononen, *Chem. Eur. J.*, 2015, **21**, 15843-15853.

146. I. S. Morgan, A. Peuronen, M. M. Hänninen, R. W. Reed, R. Clérac and H. M. Tuononen, *Inorg. Chem.*, 2014, **53**, 33-35.

147. T. N. S. Sidharth, R. Nasani, A. Gupta, B. N. S. Sooraj, S. Roy, A. Mondal and S. Konar, *Inorg. Chim. Acta*, 2020, **503**, 119395.

148. R. Nasani, T. N. S. Sidharth, S. Roy, A. Mondal, J. M. Rawson and S. Konar, *Dalton Trans.*, 2019, **48**, 14189-14200.

149. I. S. Morgan, A. Mansikkamäki, M. Rouzières, R. Clérac and H. M. Tuononen, *Dalton Trans.*, 2017, **46**, 12790-12793.

150. P. Zhang, L. Zhang and J. Tang, *Dalton Trans.*, 2015, **44**, 3923-3929.

151. P. Kaszyński, S. Kapuscinski and S. Ciastek-Iskrzycka, in *Advances in Heterocyclic Chemistry*, eds. E. F. V. Scriven and C. A. Ramsden, Academic Press, 2019, vol. 128, pp. 263-331.

152. M. Jasiński, J. Szczytko, D. Pociecha, H. Monobe and P. Kaszyński, *J. Am. Chem. Soc.*, 2016, **138**, 9421-9424.

153. M. Jasiński, S. Kapuściński and P. Kaszyński, *J. Mol. Liq.*, 2019, **277**, 1054-1059.

154. M. Jasiński, K. Szymańska, A. Gardias, D. Pociecha, H. Monobe, J. Szczytko and P. Kaszyński, *ChemPhysChem*, 2019, **20**, 636-644.

155. S. Kapuściński, A. Gardias, D. Pociecha, M. Jasiński, J. Szczytko and P. Kaszyński, *J. Mater. Chem. C*, 2018, **6**, 3079-3088.

156. K. I. Shivakumar, D. Pociecha, J. Szczytko, S. Kapuściński, H. Monobe and P. Kaszyński, *J. Mater. Chem. C*, 2020, **8**, 1083-1088.

157. M. Abe, *Chem. Rev.*, 2013, **113**, 7011-7088.

158. G. Gryn'ova, M. L. Coote and C. Corminboeuf, *WIRES Comp. Mol. Sci.*, 2015, **5**, 440-459.

159. T. Y. Gopalakrishna, W. Zeng, X. Lu and J. Wu, *Chem. Commun.*, 2018, **54**, 2186-2199.

160. K. Rishu, B. Ashima and A. Md. Ehesan, *ChemRxiv*, 2020, 10.26434/chemrxiv.12516880.v12516881.

161. P. Langer, S. Amiri, A. Bodtke, N. N. R. Saleh, K. Weisz, H. Görls and P. R. Schreiner, *J. Org. Chem.*, 2008, **73**, 5048-5063.

162. F. Wudl, P. A. Koutentis, A. Weitz, B. Ma, T. Strassner, K. N. Houk and S. I. Khan, *Journal*, 1999, **71**, 295.

163. P. Pierron, *Ann. Chim. Phys.*, 1908, **15**, 269.

164. C. P. Constantinides, G. A. Zissimou, A. A. Berezin, T. A. Ioannou, M. Manoli, D. Tsokkou, E. Theodorou, S. C. Hayes and P. A. Koutentis, *Org. Lett.*, 2015, **17**, 4026-4029.

165. Y. Zheng, M.-s. Miao, G. Dantelle, N. D. Eisenmenger, G. Wu, I. Yavuz, M. L. Chabinyc, K. N. Houk and F. Wudl, *Adv. Mater.*, 2015, **27**, 1718-1723.

166. Y. Zhang, Y. Zheng, H. Zhou, M.-S. Miao, F. Wudl and T.-Q. Nguyen, *Adv. Mater.*, 2015, **27**, 7412-7419.

167. G. A. Zissimou, A. A. Berezin, M. Manoli, C. Nicolaides, T. Trypiniotis and P. A. Koutentis, *Tetrahedron*, 2020, 131077.

168. Y. Takahashi, R. Matsuhashi, Y. Miura and N. Yoshioka, *Chem. Eur. J.*, 2018, **24**, 7939-7948.

169. X. Hu, H. Chen, L. Zhao, M. Miao and Y. Zheng, *Chem. Mater.*, 2019, **31**, 10256-10262.

170. X. Hu, H. Chen, G. Xue and Y. Zheng, *J. Mater. Chem. C*, 2020, DOI: 10.1039/D0TC00868K.

171. X. Hu, H. Chen, L. Zhao, M. Miao, J. Han, J. Wang, J. Guo, Y. Hu and Y. Zheng, *Chem. Commun.*, 2019, **55**, 7812-7815.

172. X. Hu, H. Chen, L. Zhao, M.-s. Miao, X. Zheng and Y. Zheng, *J. Mater. Chem. C*, 2019, **7**, 10460-10464.

173. X. Hu, L. Zhao, H. Chen, Y. Ding, Y.-Z. Zheng, M.-s. Miao and Y. Zheng, *J. Mater. Chem. C*, 2019, **7**, 6559-6563.

174. R. Khurana, A. Bajaj and M. E. Ali, *J. Phys. Chem. A*, 2020, **124**, 6707–6713.

175.   N. M. Gallagher, A. Olankitwanit and A. Rajca, *J. Org. Chem.*, 2015, **80**, 1291-1298.

176.   N. M. Gallagher, J. J. Bauer, M. Pink, S. Rajca and A. Rajca, *J. Am. Chem. Soc.*, 2016, **138**, 9377-9380.

177.   N. Gallagher, H. Zhang, T. Junghoefer, E. Giangrisostomi, R. Ovsyannikov, M. Pink, S. Rajca, M. B. Casu and A. Rajca, *J. Am. Chem. Soc.*, 2019, **141**, 4764-4774.

178.   A. Bajaj and M. E. Ali, *J. Phys. Chem. C*, 2019, **123**, 15186-15194.

179.   Y. Yagci, S. Jockusch and N. J. Turro, *Macromolecules*, 2010, **43**, 6245-6260.

180.   M. Chen, M. Zhong and J. A. Johnson, *Chem. Rev.*, 2016, **116**, 10167-10211.

181.   P. Chmielarz, M. Fantin, S. Park, A. A. Isse, A. Gennaro, A. J. D. Magenau, A. Sobkowiak and K. Matyjaszewski, *Prog. Polym. Sci.*, 2017, **69**, 47-78.

182.   Y. Wang, M. Fantin, S. Park, E. Gottlieb, L. Fu and K. Matyjaszewski, *Macromolecules*, 2017, **50**, 7872-7879.

183.   N. S. Hill, M. J. Fule, J. Morris, J.-L. Clément, Y. Guillaneuf, D. Gigmes and M. L. Coote, *Macromolecules*, 2020, **53**, 1567-1572.

184.   L. Zhang, E. Laborda, N. Darwish, B. B. Noble, J. H. Tyrell, S. Pluczyk, A. P. Le Brun, G. G. Wallace, J. Gonzalez, M. L. Coote and S. Ciampi, *J. Am. Chem. Soc.*, 2018, **140**, 766-774.

185.   C. L. Hammill, B. B. Noble, P. L. Norcott, S. Ciampi and M. L. Coote, *J. Phys. Chem. C*, 2019, **123**, 5273-5281.

186.   L. Zhang, R. B. Domínguez Espíndola, B. B. Noble, V. R. Gonçales, G. G. Wallace, N. Darwish, M. L. Coote and S. Ciampi, *Surfaces*, 2018, **1**, 3-11.

187.   B. B. Noble, P. L. Norcott, C. L. Hammill, S. Ciampi and M. L. Coote, *J. Phys. Chem. C*, 2019, **123**, 10300-10305.

188.   P. L. Norcott, C. L. Hammill, B. B. Noble, J. C. Robertson, A. Olding, A. C. Bissember and M. L. Coote, *J. Am. Chem. Soc.*, 2019, **141**, 15450-15455.

189.   F. J. M. Rogers, B. B. Noble and M. L. Coote, *J. Phys. Chem. A*, 2020, **124**, 6104-6110.